

Explicit Numerical Computation of Normal Forms for Poincaré Maps

Joan Gimeno^(1,*) Àngel Jorba^(1,3) Marc Jorba-Cusó^(2,3) Maorong Zou⁽⁴⁾

November 29, 2024

- (1) Departament de Matemàtiques i Informàtica, Universitat de Barcelona, Gran Via de les Corts Catalanes, 585, 08007 Barcelona, Spain, {joan,angel}@maia.ub.es
- (2) Departament de Matemàtiques, Universitat Politècnica de Catalunya, Av. Diagonal 647, 08028, Barcelona, Spain, marc.jorba@upc.edu
- (3) Centre de Recerca Matemàtica (CRM), Edifici C, Campus UAB, 0 Floor, 08193 Bellaterra, Barcelona, Spain
- (4) Department of Mathematics, University of Texas at Austin, Austin, TX 78712, USA, mzou@math.utexas.edu

* Corresponding Author

Abstract

We present a methodology for computing normal forms in discrete systems, such as those described by Poincaré maps. Our approach begins by calculating high-order derivatives of the flow with respect to initial conditions and parameters, obtained via jet transport, and then applying appropriate projections to the Poincaré section to derive the power expansion of the map. In the second step, we perform coordinate transformations to simplify the local power expansion around a dynamical object, retaining only the resonant terms. The resulting normal form provides a local description of the dynamics around the object, and shows its dependence on parameters. Notably, this method does not assume any specific structure of the system besides sufficient regularity.

To illustrate its effectiveness, we first examine the well-known Hénon-Heiles system. By fixing an energy level and using a spatial Poincaré section, the system is represented by a 2D Poincaré map. Focusing on an elliptic fixed point of this map, we compute a high-order normal form, which is a twist map obtained explicitly. This means that we have computed the invariant tori inside the energy level of the Poincaré section. Furthermore, we explore how both the fixed point and the normal form depend on the energy level of the Poincaré section, deriving the coefficients of the twist map as a power series of the energy level. This approach also enables us to obtain invariant tori inside nearby energy levels. We also discuss how to obtain the frequencies of the torus for the flow. We include a second example involving an elliptic periodic orbit of the spatial Restricted Three-Body Problem. In this case the map is 4D, and the normal form is a multidimensional twist map.

2010 Mathematics Subject Classification: 37C10, 37C27, 37C55, 37J40, 37M99, 37G05

Keywords: Normal forms; Discrete Systems; Poincaré Map; Jet Transport; Twist Map; Periodic Orbit; Parameter Dependence; Formal Power Series

Contents

1	Introduction	3
2	Preliminaries	4
2.1	Jet transport	4
2.2	Nested jets	7
2.3	Taylor expansion of implicit functions	7
2.4	On parameter-dependence eigenpairs	9
3	Normal forms on discrete dynamical systems	10
3.1	Semi-analytical construction of a normal form	10
3.2	Polynomial composition and reverse maps	12
3.3	Normal form with respect to parameters	12
4	Frequency recovery from a Poincaré map	13
4.1	Visualization of tori	17
5	Explicit torus construction on elliptic Hamiltonian points	18
5.1	Construction of high-dimensional twist maps	18
5.1.1	Example: twist map in the plane	20
5.2	Effective computation of invariant tori	20
5.3	Tori construction from frequency recovery	20
6	Experiments	21
6.1	The Hénon-Heiles system	22
6.1.1	Computation of a fixed point	22
6.1.2	Computation of a curve of fixed points parametrized by the energy	22
6.1.3	Total power expansion at the fixed point curve	23
6.1.4	Normal form and twist map around the fixed point curve	25
6.1.5	Invariant curve and torus frequencies	26
6.1.6	Full torus visualization	27
6.2	The Restricted Three Body Problem	27
6.2.1	Elliptic fixed point	29
6.2.2	Normal form and twist construction	29
6.2.3	Torus visualizations	31
	References	33

1. Introduction

The study of dynamical systems has traditionally involved simplifying complex systems to make them more manageable for analysis. A key tool in this process is the computation of normal forms, which simplify dynamical systems by reducing them to their essential elements through change of coordinates. This technique is commonly applied to understand the local behaviour of systems near invariant structures such as equilibrium points or periodic orbits. Generally, a normal form process consists of a series of changes of variables that transforms the Taylor expansion of a vector field (or a map) up to a certain order according to some criteria. Dependence of parameters is often included when normal forms are used to analyze bifurcations of equilibrium (or fixed) points.

In Hamiltonian systems, specialized methods dealing directly with Hamiltonian functions have been developed. Notably, Birkhoff and Kolmogorov normal forms [Bir27, Mos68, Arn78, Bru88], have proven invaluable, especially for studying the dynamics in a neighbourhood of equilibrium points (i.e. bifurcations, non-linear stability and KAM theory [Kol54]). Technique based on manipulating the Hamiltonian function has been extended to cope also with expansions about periodic and quasi-periodic orbits via a combination of Floquet Theory and Taylor-Fourier series [GJ04, GJ05, GJL05, JV98, And02, JJCR20]. However, applying Floquet Theory in autonomous Hamiltonian systems, where periodic orbits occur in families, can lead to particularly cumbersome coordinate transformations. These additional complexities are well-documented in [JV98], in contrast to other studies that focus on isolated periodic orbits (examples of isolated periodic orbits are the dynamical equivalents of equilibrium points of a periodically perturbed autonomous system).

In this paper, we approach the computation of normal forms about periodic orbits via the Poincaré map. The periodic orbit is seen as a fixed point of the Poincaré map and one can avoid dealing with the Floquet Change of variables when computing the linear terms of the normal form. Although the examples in this paper focus on periodic orbits of Hamiltonian systems, our method does not assume any specific structure, such as Hamiltonian or symplectic properties, beyond regularity assumptions. This generalization makes the approach applicable to a broader range of systems, including those that are dissipative or non-Hamiltonian, thus enhancing its utility across various fields of study and a wide variety of systems.

The Poincaré map, first introduced by Henri Poincaré in [Poi99], reduces the dimension of a continuous system by capturing the intersections of a trajectory with a chosen section. This reduction allows for the study of complex systems in a lower-dimensional space, making it easier to analyse the local dynamics. Our method leverages this dimensional reduction by first computing high-order derivatives of the system using jet transport and project them to the section, based on the recent methodology in [GJJC⁺23]. This approach provides a more detailed representation of the system's local behaviour around the dynamical object, making the analysis more manageable.

Subsequently, the algorithm performs coordinate transformations to simplify the local representation, retaining only the essential resonance terms. This procedure, which includes formal power expansions and techniques based on the Implicit Function Theorem, systematically reduces the complexity of the system while preserving the key dynamical features necessary for understanding the system's behaviour. By removing non-resonant terms, the method provides a clearer, more focused view of the dynamics near critical points, allowing for more efficient analysis.

A key contribution of this work is its robust performance under parameter dependence. The method is designed to handle changes in system parameters without losing accuracy or stability, making it particularly useful for studying families of systems or systems with external perturbations. This flexibility sets it apart from classical approaches, which may struggle to accommodate such variations by introducing model-dependent procedures.

To demonstrate the effectiveness of the proposed method, we apply it to the explicit construction of high-dimensional twist maps, a type of dynamical system where the twist condition ensures quasi-periodic motion. As a by-product of this construction, we introduce a general frequency recovery method for high-

dimensional tori, which is then used to fully visualize these twist maps and their tori. This development not only showcases the practical utility of the method but also contributes to the broader understanding of multi-dimensional dynamical systems.

In summary, this paper introduces a comprehensive, systematic method for computing normal forms in discrete systems without relying on specific structural assumptions. By utilising high-order derivatives, jet transport, and resonance-preserving transformations, this method offers a powerful and flexible tool for the study of both classical and modern dynamical systems.

This paper is organized as follows. We begin with a self-contained discussion of preliminary tools in Section 2. We then present the detailed normal form procedure in Section 3. Section 4 is devoted to study the frequency recovery of a torus from a Poincaré map. Following that, Section 5 uses the normal form procedure to describe the torus construction of an elliptic point and how to recover the frequency from it. Finally, Section 6 provides some examples to illustrate the normal form computation as well as the torus construction.

2. Preliminaries

The numerical computation of the normal forms in this work relies on several preliminary tools, which can be studied independently. The common problem is to compute infinitesimal expansions in different settings. These computations are done using automatic differentiation to obtain numerical high-order derivatives. When applied to an ODE solver, automatic differentiation results in a technique called jet transport. In [GJJC⁺23], it is proved that jet transport is equivalent to solving high order variational equations. In Section 2.1 we explain the jet transport concept and generalize the results in [GJJC⁺23].

In the example developed in Section 6.1 we compute the Kolmogorov normal form about a fixed point of a certain Poincaré map, also taking into account the dependence on the Hamiltonian (which in this paper is considered an internal parameter). This approach is used to capture an open set of the phase space (if the energy is kept fixed, the normal form only captures a codimension one neighbourhood of the fixed point). Considering parameter dependence involves extra steps in our algorithm, namely:

- i) The dependence of fixed points on the energy needs to be of high order. As the fixed point can be obtained as an implicit function of an equation, we can combine the Implicit Function Theorem and the parameterization method (see [CFdIL05]) to compute the Taylor expansion of the fixed point with respect to the parameter. In section 2.3 we explain how this can be achieved.
- ii) The variational equations have to be solved also with respect to parameters. The parameter is internal (is a function of the phase variables) and typically, the dependence of the fixed point with respect to the parameter is required up to low order (comparatively speaking to the order of the normal form). Then, it is advisable to be able to solve variational equations with a different prescribed order for the parameter. This is achieved by using an arithmetic of nested jets, i.e., jets with symbols represent the derivatives with respect to the phase variables whose coefficients are jets with symbols representing the derivative with respect the parameter. This is covered in Section 2.2.
- iii) The eigendecomposition problem of the linear stability of the fixed point must also be obtained with respect to the parameter. In Section 2.4 we summarize briefly the techniques [Sun85, Sun90] that solve the problem.

2.1 Jet transport

The concept of jet was firstly introduced by Charles Ehresmann in 1951, see [Ehr51]. Given $\alpha: \mathbb{R}^s \rightarrow \mathbb{R}^m$ be an ℓ -th continuously differentiable map, defined in a subset of \mathbb{R}^s). Its ℓ -jet is a map that provides a correspondence between a point x_0 and α and the Taylor polynomial of order ℓ expanded about x_0 . That is:

$$J_{x_0}^\ell[\alpha](\delta) = \sum_{j=0}^{\ell} \alpha_j(\delta), \quad \alpha_j(\delta) \stackrel{\text{def}}{=} \sum_{|k|=0}^j a_k \delta^k, \quad a_k = \frac{1}{k_1! \cdots k_s!} \frac{\partial^k \alpha}{\partial \delta_1^{k_1} \cdots \partial \delta_s^{k_s}}(x_0), \quad (1)$$

where $a_k \in \mathbb{R}^m$, $\delta = (\delta_1, \dots, \delta_s)$ is a set of s symbols, $k = (k_1, \dots, k_s) \in \mathbb{N}^s$ is a multi-index, $|k| \stackrel{\text{def}}{=} k_1 + \cdots + k_s$, and $\delta^k \stackrel{\text{def}}{=} \delta_1^{k_1} \cdots \delta_s^{k_s}$. As in the classical Taylor polynomial, the combinatorial terms involving the multi-index k in a_k are due to repetitions of the crossing derivatives. The point x_0 is, typically, called the **source** and $\alpha(x_0)$ the **target** of the Jet.

Remark 1 (about an heuristic range of validity). We consider the set of symbols δ in (1) as a formal variable to operate with, or as an “indeterminate” with no specific value. However, in practice, many times it is also convenient to quantify the range of values of δ . Thus, if $\alpha = (\alpha^1, \dots, \alpha^m)$ denotes the coordinate maps, we define the *validity range* of the jet $J_{x_0}^\ell[\alpha](\delta)$ in (1) with tolerance ϵ as a number δ_{\max} on the uniform hypercube $\delta \in [-\delta_{\max}, \delta_{\max}]^s$ given by the formula

$$\delta_{\max} = \delta_{\max}(\epsilon; J_0^\ell[\alpha](\delta)) \stackrel{\text{def}}{=} \min_{i=1, \dots, m} 10^{\nu_i}, \quad \nu_i \stackrel{\text{def}}{=} \max \left\{ \frac{\log_{10}(\epsilon) - \log_{10} |\alpha_{\ell-1}^i(\delta)|}{\ell-1}, \frac{\log_{10}(\epsilon) - \log_{10} |\alpha_\ell^i(\delta)|}{\ell} \right\}. \quad (2)$$

The formula (2) is heuristic, and it is motivated by the square root test for the convergence of a power series, which states that the ℓ -square root of the ℓ th coefficient tends to the inverse of the convergence radius of the series. Thus, our choice of δ_{\max} comes from isolating $|\delta|$ in the inequality $|\alpha_j^i(\delta)| \leq \epsilon$ for $j \in \{\ell-1, \ell\}$. We define the *safety validity range* δ_\star as the validity range multiplied by a safety factor, e.g. $\delta_\star \stackrel{\text{def}}{=} 0.95\delta_{\max}$. This heuristic number δ_\star can be used to scale the jet and prevent numerical overflow/underflow. In particular, we will use it to scale the output of the normal form algorithm, see Remark 10.

Given two differentiable maps $\alpha: \mathbb{R}^s \rightarrow \mathbb{R}^m$ and $\beta: \mathbb{R}^m \rightarrow \mathbb{R}^r$, the composition of jets satisfies the following equality up to order ℓ

$$J_{\alpha(x_0)}^\ell[\beta] \circ J_{x_0}^\ell[\alpha](\delta) = J_{x_0}^\ell[\beta \circ \alpha](\delta). \quad (3)$$

It is straightforward (by Schwarz’s lemma) that if $t \mapsto \alpha_t$ is differentiable, then the derivative with respect to t of the jet is the jet of the derivative, i.e.

$$\frac{\partial}{\partial t} J_0^\ell[\alpha_t](\delta) = J_0^\ell \left[\frac{\partial}{\partial t} \alpha_t \right](\delta). \quad (4)$$

Given a point $x_0 \in \mathbb{R}^n$ we will denote by $\mathcal{J}_{x_0}^{\ell,s}(\mathbb{R}^m)$ the set of all jets with seed x_0 of order ℓ and s symbols. This leads to a compact writing of the variational equations.

Definition 2 (ℓ -th jet differential equation). Given fixed integers $\ell, s \geq 1$, let $\{x(t)\}$ be the solution of a smooth initial value problem $\dot{x}(t) = f \circ x(t)$ and $x(0) = x_0$ in \mathbb{R}^n . If $X: \mathbb{R} \rightarrow \mathcal{J}_{x_0}^{\ell,s}(\mathbb{R}^n)$, we define the ℓ -th order jet differential equation as

$$\dot{X}(t) = J_{x(t)}^\ell[f] \circ X(t). \quad (5)$$

The ODE system (5) is defined on the space of jets of order ℓ , in particular, the equality in (5) must be interpreted in such a space. Note that the number of symbols s and the order ℓ can be arbitrary but they must be fixed to define (5).

Any initial condition of $X(0) \in \mathcal{J}_{x_0}^{\ell,s}(\mathbb{R}^n)$ gives an admissible initial value problem. A solution $X(t)$ is a jet that is transported jointly with the trajectory $x(t)$. The exact interpretation of the jet $X(t)$ will depend on the initial jet value $X(0)$, the symbols δ , and the order ℓ .

Following the notation in (1), the equation associated to X_j is called variational equation of order j ($j < \ell$). Computing of X_j requires X_i , for $i = 0, \dots, j - 1$.

Theorem 3 proves that the jet associated to the flow of an ODE can be seen as an ODE system in the space of jet of the form (5). In particular, when $X(0)(\delta) = x_0 + \delta$ for $s = n$ symbols, then $X(t)$ corresponds to the high-order derivative up to order ℓ of the time t map at x_0 .

Theorem 3. *Let $\{x(t)\}$ be the solution of the smooth initial value problem $\dot{x}(t) = f \circ x(t)$ with $x(0) = x_0$ in \mathbb{R}^n . Then $X(t) = J_{x_0}^\ell[x(t)]$ satisfies (5).*

Proof. Using (4), $x(t)$ is a solution, and (3), we derive

$$\frac{\partial}{\partial t} J_{x_0}^\ell[x(t)] = J_{x_0}^\ell \left[\frac{\partial}{\partial t} x(t) \right] = J_{x_0}^\ell[f \circ x(t)] = J_{x(t)}^\ell[f] \circ J_{x_0}^\ell[x(t)]. \quad \square$$

Theorem 3 provides a systematic way to compute high-order variational flows, thereby providing a neighbourhood approximation of the orbit $\{x(t)\}$. Indeed, if a numerical stepper of an ODE in \mathbb{R}^n performs its operations in the space of jets, then the same numerical stepper as for the ODE in \mathbb{R}^n but with jet operations will be able to provide the derivatives of the flow with respect to the initial conditions. This was proved in detail in [GJJC⁺23] for some families of numerical steppers and more recently in [PF23] for generalized linear integrators.

It is important to emphasize that the method described in [GJJC⁺23] is different from others, such as those applied to specific ODE models, methods based on numerical differentiation and its extrapolation to higher orders, or approaches that use symbolic differentiation of the vector field f to explicitly construct the system (5), see [ABBR12].

The method in [GJJC⁺23] is quite general, relying on automatic differentiation (AD) to implicitly evaluate a system of the form (5) without explicitly generating the full expression. AD offers a computational approach to perform derivative evaluation of an algorithm, provided it can be represented by a combination of elementary expressions. AD has already been applied successfully in different areas such as in dynamical systems [HCL⁺16, PP15] and in more general settings [GC91].

Forward AD is used to obtain high-order derivatives of the output of an algorithm with respect to its input. Computationally, this is achieved by replacing the standard arithmetic of real numbers with truncated formal power series arithmetic, which encodes these high-order derivatives – referred to as *jet*. In conjunction with numerical integration of a differential equation the jet is transported through the solution of the equation, leading to the concept of *jet transport*. The output is a truncated power series that contains the trajectory and the high-order derivatives with respect to the initial inputs. These approach has been used in several papers [Mur20, JN21, GJNO22].

The Taylor expansion of the flow can also be computed by differentiating symbolically the original vectorfield to obtain the variational equations up to high order and then solving them numerically. The main takeaway of Theorem 3 is that both approaches are exactly the same (if the same method to solve the ODE is used). Notice that, the symbolic approach produces a number of repeated equations (due to crossing derivatives) that have to be collected in a suitable way. In the jet transport approach, where the derivatives are automatic (or semi-analytic), this problem is solved by collecting repeated terms at each operation of the polynomial arithmetic (see [Knu98]). Recently, the public software [JZ05] has been enhanced to support jet transport [GJZ22].

The procedure outlined in Algorithm A is also applicable to discrete systems that depend on parameters under suitable considerations. Specifically, we need the invariant object to be given depending on such parameters. Section 2.3 describes such a procedure, leveraging the implicit function theorem. The key point is that the different terms involved can be obtained systematically by using the automatic differentiation and jet transport.

Once a local truncated expansion of the invariant object with respect to parameters is obtained, a local representation in the phase space is required. Section 2.2 introduces a new arithmetic that saves computation of coefficients and allows to obtain a local representation with different levels of accuracy.

Finally, we verify that the new arithmetic works well with the Algorithm A. Section 2.4 addresses the only remaining consideration: the eigen-decomposition of the matrix appearing in the step 3.

2.2 Nested jets

The paper [GJJC⁺23] proves that the use of jet transport of an ODE is the same as computing high-order variational equations. In particular, the result applies to Poincaré maps, which under generic assumptions are (local) diffeomorphisms. These maps describe discrete dynamical systems given by an underlying ODE. The input of these maps are an initial condition and the output are the solution of the ODE at a final time of the trajectory. That final time can be either known or unknown. In the first case, the map is called stroboscopic Poincaré map and in the second case, spatial Poincaré map. The later fixes a section, say Σ , in the state space such that starting with an $x \in \Sigma$, it integrates $T(x)$ units of time until the ODE-solution lies in Σ after crossing a finite number of times such a section.

We denote the discrete dynamical system associated to a Poincaré map as

$$\bar{x} = P(x; T(x), \lambda), \tag{6}$$

where the $T(x)$ denotes the final time of integration (possibly depending on x) and λ denotes a parameter of the system. Here, we use the semicolon notation ; to indicate the arguments that follow are either parameters or depend on previous arguments. Note that one can always extend the phase space of the ODE to incorporate the dynamics of the parameter, with $\dot{\lambda} = 0$; however the discrete system (6) would remain the same. A straightforward application of jet propagation with all the variables of the system could result in the generation of unnecessary coefficients, making the process optimizable.

A key distinction when T depends on x is the need to correct the output by performing projections onto the section Σ . This required step is not possible for all numerical integrators, as it is limited by the order of the numerical stepper. In simple terms, the idea is to add a symbol, say s , in the input data x and evaluate P at $x + s$. As a consequence, one must compute $T(x + s)$. It is an infinitesimal correction of the ODE-flying time. These corrections can be computed by ensuring that $P(x + s; T(x + s), \lambda)$ belongs to Σ . They depend on the geometry of Σ and in [GJJC⁺23] formulas and procedures for this process were discussed when Σ is an affine hyperplane.

It is also interesting to compute high-order derivatives with different orders. Indeed, suppose we compute a dynamical object of (6) up to a certain order, say m_s , while simultaneously expressing the object in a neighbourhood of the parameter λ . This requires a formal power series expansion around λ ; or equivalently, to introduce a symbol u and evaluate at $\lambda + u$ instead of λ . For performance reasons, these two neighbourhoods may have different accuracy levels. More formally, if s and u denote two set of symbols, then we need to compute

$$P(x + s; T(x + s), \lambda + u)$$

with exponents on u up to m_u and on s up to m_s . This problem is addressed by considering power series whose coefficients are also truncated power series. Proper adjustments to the stepsize control ensure that the jet transport still provides the required high-order variational needed to compute the high-order derivatives of P . This process has recently been systematized in the software package [GJZ22] optimizing to some set of symbols and orders in the jets.

2.3 Taylor expansion of implicit functions

In certain contexts, the procedure for obtaining an invariant object must satisfy an implicit equation. In such cases, it is often possible to construct a recursive algorithm that compute the expansion order-by-order. The recursive methods can be stopped at a prescribed order, and the resulting output can then serve as the input for a Newton-like algorithm to compute a set of new coefficients expansion all at once.

Let $F: \mathbb{R}^n \times \mathbb{R} \rightarrow \mathbb{R}^n$ be a smooth function for which there exist a pair $(x_0, 0)$, $x_0 \in \mathbb{R}^n$, such that

$$F(x_0, 0) = 0.$$

Then, the Implicit Function Theorem states that, provided that $D_x F(x_0, 0)$ is invertible, there exists a smooth locally defined implicit function $u \mapsto x(u)$ such that

$$F(x(u), u) = 0, \quad (7)$$

for each u in neighbourhood of 0. In particular, as long as F is differentiable, then we can consider the first derivative of the implicit function. Moreover, we can compute it. Differentiating equation (7) with respect to the second variable, u , leads to the following expression:

$$\frac{d}{du} F(x(u), u) = D_x F(x(u), u) \frac{d}{du} x(u) + \frac{\partial}{\partial u} F(x(u), u) = 0.$$

Evaluating the last equation at $u = 0$ we obtain a formula for the first derivative at $u = 0$

$$x_1 := \frac{d}{du} x(0) = -[D_x F(x_0, 0)]^{-1} \frac{\partial}{\partial u} F(x_0, 0).$$

If F is a smooth function, then x can be Taylor-expanded around the origin. Notice that, we already have the linear expansion:

$$x^{[1]}(t) = x_0 + x_1 u.$$

Again, equation (7) provides a way to compute recursively, higher terms of the Taylor expansion of the implicit function x . Let us assume that we have already computed an expansion of order ℓ and let us see how to obtain order $\ell + 1$. That is, suppose we have

$$x^{[\ell]}(u) = \sum_{k=0}^{\ell} x_k u^k.$$

If we evaluate and use equation (7), we get

$$F \left(\sum_{k=0}^{\ell} x_k u^k + x_{\ell+1} u^{\ell+1}, u \right) = 0,$$

where the coefficients $x_0, x_1, \dots, x_{\ell}$ are all already known while $x_{\ell+1}$ is not. Now, we expand the last equation but only minding the terms of order $\ell + 1$ or less. We have

$$F \left(\sum_{k=0}^{\ell} x_k u^k, u \right) + D_x F \left(\sum_{k=0}^{\ell} x_k u^k, u \right) x_{\ell+1} u^{\ell+1} + \mathcal{O}(u^{\ell+1}) = 0.$$

Now, we name the expansion

$$F \left(\sum_{k=0}^{\ell} x_k u^k, u \right) = \sum_{k=0}^{\ell+1} F_k u^k.$$

Then, the $(\ell + 1)$ -th term can be isolated easily:

$$x_{\ell+1} = -[D_x F(x_0, 0)]^{-1} F_{\ell+1}.$$

Remark 4. In our examples, we are going to consider fixed points of Poincaré maps constructed in a spatial section. Therefore, the procedure described here will also provide a local expansion with respect to the parameters of the period. See Section 6.1.2 later on.

Remark 5. The procedure also admits the use of scaling factor. This involves in scaling the symbol u by a factor ϱ , called *scaling factor*. The goal is to minimise the error propagation by preventing the norms of the coefficients from growing or shrinking too rapidly with the order. For example, see [Ric80, FdIL92, GJNO22]. Typically, the procedure is run twice: first up to a specified order, to estimate ϱ (e.g. by using the square root test), and then it is run again, this time multiplying the x_1 coefficient by ϱ . As a result, the iterative process scales all subsequent coefficients x_k .

2.4 On parameter-dependence eigenpairs

An application of Section 2.3 is the computation of power series expansion of the eigenvalue problem. Let $A(u)$ be a power series in the variable u whose coefficients are n -by- n square matrices. Let us consider the eigenvalue problem associated to $A(u)$ which gives as an output power expansions for the eigenvalue problem at $u = 0$. In the following, we give a brief summary of [Sun85, Sun90] where they investigated sufficient spectrum conditions on $A(0)$ that allow for the computation of such an expansion.

Let v_i be a right eigenvector and let w_i be a left eigenvector of the eigenvalue μ_i of $A(0)$. That is, they satisfy

$$A(0)v_i = \mu_i v_i \quad \text{and} \quad w_i^H A(0) = w_i^H \mu_i,$$

where $(\cdot)^H$ denotes the conjugate transpose.

Let us assume that μ_1 is simple, i.e. $\mu_1 \neq \mu_i$ for $i \neq 1$. If $V = (v_i)$ and $W = (w_i)$ are the matrices with columns v_i and w_i respectively normalised as $w_i^\top v_i = 1$, then

$$W^H A(0)V = \begin{pmatrix} \mu_1 & \\ & M_2 \end{pmatrix}, \quad M_2 \stackrel{\text{def}}{=} \text{diag}(\mu_2, \dots, \mu_n).$$

Let us compute the expression

$$W^H A(u)V = \begin{pmatrix} a_{11}(u) & a_{12}(u)^\top \\ a_{21}(u) & A_{22}(u) \end{pmatrix}.$$

Then we apply Section 2.3 with the function

$$F(z, u) \stackrel{\text{def}}{=} a_{21}(u) + (A_{22}(u) - a_{11}(u)I_{n-1})z - za_{12}(u)^\top z$$

to find $z(u)$. Here we can either use an ad-hoc implementation that evaluates $F(z, u)$ with jets or use the new arithmetic of jets of jet described in Section 2.2; that is jets of $n - 1$ symbols and degree 2 with coefficients being jets of as many symbols of u and degree as those in $A(u)$. We need $M_2 - \mu_1 I_{n-1}$ to be invertible, which holds due to the assumption of simple eigenvalue μ_1 . Therefore, after computing $z(u)$, we have

$$\mu_1(u) \stackrel{\text{def}}{=} a_{11}(u) + a_{12}(u)^\top z(u), \quad v_1(u) \stackrel{\text{def}}{=} v_1 + V_2 z(u),$$

with $V_2 \stackrel{\text{def}}{=} (v_2 \ \dots \ v_n)$. Thus, $\mu_1(u)$ and $v_1(u)$ satisfy $A(u)v_1(u) = \mu_1(u)v_1(u)$.

Remark 6 (normalization condition). All eigenvalue problem is unique up to scaling of its eigenvector. Here we fix this lack of uniqueness by imposing $w_i^\top v_i = 1$. Standard eigen-decomposition software routines may not ensure this normalization and in such a case, we can always scale either w_i or v_i with $w_i^\top v_i$.

Remark 7 (complex eigenvalue). Note that if $(\mu_1(0), v_1(0))$ is a complex simple eigenpair (in the complex eigen-decomposition), then the parameter-dependence solution of its conjugate $(\overline{\mu_1(0)}, \overline{v_1(0)})$ will simply be the conjugate expansions, i.e. $\overline{\mu_1}(u) = \overline{\mu_1(u)}$ and $\overline{v_1}(u) = \overline{v_1(u)}$.

Remark 8 (about the simplicity assumption). The construction of the parameter dependence of an eigenpair relies heavily on the assumption that the eigenvalue is simple. This assumption is essential for applying the Implicit Function Theorem to the function F . In fact, if $\|u\|$ is sufficiently small, the new parameterized eigenvalue will also be simple, as noted in [Wil65]. However, when dealing with multiple eigenvalues, the theory becomes more complex due to the loss of regularity. For a general approach, see [Kat66] or for the case of real multiple eigenvalues, refer to [Bro79].

3. Normal forms on discrete dynamical systems

A normal form is a (local) simplified representation of a dynamical system that retains and reflects the system's behavior. The algorithm we present assumes a discrete dynamical system $\bar{x} = P(x)$, which may depend on parameters and is defined on a suitable subset of \mathbb{R}^n . We also assume that the system is at least finite continuously differentiable.

In our experiments, as well as in some of the sections, we assume the discrete system arises from the flow of an underlying ODE system. After a specific integration time, the flow produces the discrete system. We assume this discrete system has a fixed point, i.e. $P(x_0) = x_0$ which corresponds to a periodic orbit of the continuous dynamical system. Notice that this setup trivially includes the normal form of an equilibrium point. Moreover, a similar procedure can be adapted to the case of closed curves, which corresponds to quasi-periodic solution, as discussed in [GJNO22]. However, for clarity of exposition, we will not formalize it here and hope to address it in the future.

Normal forms are classified based on the resonance terms that survive after applying the normal form procedure. In sufficiently smooth systems, the Poincaré-Dulac Theorem, [Arn83] proves that, locally, any discrete system is formally equivalent to a formal discrete dynamical system only containing resonant monomials. Hence, the procedure begins with obtaining a local expression of the solutions around the fixed point, generically, by a Taylor expansion. Following this, a finite sequence of coordinate transformation is applied, with each iteration either eliminating or revealing a term in the normal form based on resonance.

The transformations in the procedure must produce equivalent dynamical systems. Specifically, a (dynamical) system G_1 is equivalent to G_2 when there exists a (smooth) change of coordinates c_1 such that $G_1 \circ c_1 = c_1 \circ G_2$. Thus, what we will do is to build a sequence of equivalent dynamical systems G_k , each with their corresponding change of coordinate c_k such that $G_{k+1} = c_k^{-1} \circ G_k \circ c_k$. In each iteration k , the new system is either simplified, or a resonance term is revealed and must be preserved for the next iteration. The process finishes after a predetermined finite number of iterations.

In general, the process done up to order k will not guarantee a convergent result, i.e. the terms beyond k may still leads to a divergent expansion. Nevertheless, the truncated expansion will have an asymptotic behaviour and the transformed expansion up to order k will only contain resonance terms and it will standardize the dynamical system in a small neighbourhood.

3.1 Semi-analytical construction of a normal form

Algorithm A describes a systematic procedure to compute high-order terms of a normal form of a discrete dynamical system. The algorithm assumes as input a fixed point of the discrete dynamical system, which, if derived from an underlying ODE, may represent an equilibrium or a periodic orbit. For clarity of exposition, we will assume the latter case, as it includes the equilibrium case.

The algorithm assumes that one is able to compute a local expansion around the fixed point; which means, in case of an ODE, to integrate high-order variational equations, see Section 2.1.

Pseudo-Algorithm A (Normal form construction of a fixed point of a discrete dynamical system).

★ **Input:** Fixed point x_0 of a Poincaré map $P: U \subset \mathbb{R}^n \rightarrow \mathbb{R}^n$ and scaling factor ϱ (by default 1)

★ **Output:** Changes of coordinates $c_0, c_1, \dots, c_k, \dots$ and normal form around x_0

1. $G(s) \leftarrow P(x_0 + s) = \sum_{|k| \geq 0} \sum_{|j|=k} G_j s^j$ obtained by a jet transport process at x_0

2. $c_0(s) \leftarrow x_0 + s$

3. Let V and D be matrices over \mathbb{C} of eigenvectors and eigenvalues of $G_{|j|=1}$ respectively, i.e.

$$D = V^{-1} G_{|j|=1} V = \begin{pmatrix} \Lambda_1 & & \\ & \ddots & \\ & & \Lambda_n \end{pmatrix}$$

4. $c_1(s) \leftarrow (\varrho V)s$

5. $F^1 \leftarrow (c_0 \circ c_1)^{-1} \circ G \circ (c_0 \circ c_1)$

6. For $k = 2, 3, \dots$

6.a) $c_k(s) \leftarrow s - \sum_{|j|=k} b_j s^j$ with

$$b_{j,i} = \frac{F_{j,i}^{k-1}}{\Lambda_i - \Lambda^j}, \quad \Lambda^j \stackrel{\text{def}}{=} \Lambda_1^{j_1} \dots \Lambda_n^{j_n}, \quad i = 1, \dots, n$$

$b_{j,i} \leftarrow 0$ if $\Lambda_i - \Lambda^j$ is close to zero (resonance case)

6.b) $F^k \leftarrow c_k^{-1} \circ F^{k-1} \circ c_k$.

Algorithm A is justified as long as the matrix D is diagonal, which may require using complex numbers. Indeed, the change of coordinate c_k corrects the order k and its inverse has the form

$$c_k^{-1}(s) = s + \sum_{|j|=k} b_j s^j + O(|s|^{2k-1}).$$

Assume we have applied the algorithm $k - 1$ times and let us try step k . The F^{k-1} (in absence of resonances) will only have the first order and orders higher than or equal to $k - 1$, that is,

$$F^{k-1}(s) = Ds + \sum_{|j|=k} F_j^{k-1} s^j + O_{k+1}.$$

Then the F^k resulting from the conjugacy c_k will have the form

$$F^k(s) = c_k^{-1} \circ F^{k-1} \circ c_k(s) = Ds + \sum_{|j|=k} (F_j^{k-1} - Db_j) s^j + b_j \cdot (Ds)^j + O_{k+1},$$

where O_{k+1} denotes higher-order terms. Since D is a diagonal matrix, the choice of b_j leads to zero coefficients for $|j| = k$.

Let us now highlight some key points regarding the general procedure.

Remark 9 (eigenvalues). The algorithm assumes at step 3 that first derivative of the diffeomorphism at x_0 diagonalizes with possibly complex number. Degenerate cases exist and ad-hoc procedures may be needed, especially when the denominator in step 6a becomes very small.

Remark 10 (scaling factor). The normal form we compute follows a semi analytical construction in the sense that it does not guarantee decay with each iteration. When fixed an iteration, say N , we can estimate the decay of part of the coefficients and use that as the scaling factor ϱ to control the growth of the coefficient norms, preventing them from exceeding arithmetic accuracy. This involves re-running the procedure with the estimated ϱ .

Remark 11 (resonance treatment). Algorithm A keeps the resonant terms at step 6a. By setting $b_{j,i} = 0$ that coefficient will not be turned to zero when computing F^k at step 6b.

Remark 12 (storage of the changes of coordinates). The changes of coordinates c_0, c_1, \dots, c_k have a very particular form, that is, just x_0 for c_0 , V for c_1 , and b_j for $|j| = k$ in c_k . These terms plus the identity when $|j| = 1$ for $k \neq 1$ are the only possible non-zero terms of the changes of coordinates. Thus, all the c_0, \dots, c_k can be stored in just one power series up to order k . An ad-hoc code to perform the evaluation action of $c = c_0 \circ \dots \circ c_k$ can be implemented effectively without computing explicitly the composition of power series.

Remark 13 (correctness test). To check whether the final transformed dynamical system is accurate, one performs a test that certifies that the order of the power series is the requested one. Let $a \in \mathbb{R}^n$ with $\|a\| = h$ and let $F^k = c^{-1} \circ G \circ c$ where $c \stackrel{\text{def}}{=} c_0 \circ \dots \circ c_k$. If

$$e_h = \|c \circ F^k(a) - G \circ c(a)\|,$$

then $\log_2(e_h/e_{h/2}) \approx k + 1$. Note that the test may not work for all h or k due to numerical cancellations and limitations in the numerical representation of numbers.

Remark 14 (computational complexity). The most computationally intensive step in Algorithm A occurs at the beginning, during the computation of $G(s)$. This step involves calculating high-order derivatives of the Poincaré map P , which can be highly nonlinear and may require computing a flow map. The remaining steps consists primarily of algebraic manipulation of jets. See Section 6 for some timing reports.

Remark 15 (multiple shooting). If the P is described as r equidistance multiple shooting, then the dimension of the fixed point x_0 consists in multiple copies of each intermediate section and the eigenvalues are r th root of unit, as described in [GJNO22] and earlier works. In particular, the resonance treatment in the step 6a becomes the same.

3.2 Polynomial composition and reverse maps

The performance of Algorithm A is dominated by step 6b which involves composition and reversion of truncated power series. These operations have already being addressed in the 1-symbol case by classical authors like Thacher [Tha66], Brent [BK78], and Knuth [Knu98, §4.7]. Different authors have provided several versions including recursive and iterative schemes. [PP15] compared these schemes and concluded that a recurrent scheme is, generically, faster for higher orders. Our algorithm operates with an arbitrary, though finite, number of symbols.

The inversion c_k^{-1} can easily be computed in our case. Trivially, $c_0^{-1}(s) = -x_0 + s$, $c_1^{-1}(s) = V^{-1}s$, and for $k \geq 2$ what we really need to compute is not c_k^{-1} but its composition with $(F^{k-1} \circ c_k)$, called the general power series reversion. More precisely, let $q(s)$ be a power series. Then to compute $c_k^{-1} \circ q(s)$ we need to find the coefficients of $h(s)$ such that $c_k \circ h = q$, that is,

$$h(s) - \sum_{|j|=k} b_j(h(s))^j = q(s), \quad (8)$$

which is solved by power matching as long as $q(0) = 0$. We always have that the first order homogeneous polynomials coincide, i.e., $h_1 = q_1$ and thus we start solving from the order 2.

If we have m_s symbols in s , then the algorithm that solves (8) only needs $2m_s + 1$ power series of storage. Its performance is dominated by the composition operator which in the worst case is $O(N^2)$, where N is the order of the truncated power series. The new release in [GJZ22] provides a numerical implementation for composition and reverse functions of truncated power series for arbitrary number of symbols and degrees that we use for this paper.

3.3 Normal form with respect to parameters

Algorithm A can also be adapted to compute local power expansion of the normal form with respect to a parameter, with some modifications. These changes begins with the input, where the fixed point x_0

must now be provided as a map $u \mapsto x_0(u)$. This adaptation requires the use of Section 2.2 to obtain a formal power expansion of the fixed point in terms of the parameter λ . Specifically, it involves applying Section 2.3 to the fixed point condition.

The remaining steps consists of adapting the procedure to the new setting. Specifically, *i*) the jet transport process for computing G will now involve jets of different orders to compute $G(s, u) \leftarrow P(x_0 + s, \lambda + u)$, as detailed in Section 2.2; *ii*) the eigen-decomposition in step 3 will require methods in Section 2.4; *iii*) the composition of reverse map in Section 3.2 will become straightforward using arithmetic of jets of different orders; *iv*) the resonance condition in step 6a will essentially be the same, with the only adjustment being that for nearby resonance with respect to u , the power expansion on u might have a reduced validity range; and *v*) an additional scaling factor ϱ_u can be introduced to scale the expansion on the symbol u .

4. Frequency recovery from a Poincaré map

Using explicit normal forms in Poincaré maps enables us to compute quasi-periodic solutions that reside within invariant tori. It also allows us to recover all the frequencies associated with that torus sliced by a section on the Poincaré map. This capability enhances the study of quasi-periodic solutions to ordinary differential equations, providing crucial insights into the structural and geometric properties of dynamical systems.

This is particularly significant in the context of Hamiltonian systems. In integrable systems, quasi-periodic motion fills the phase space, providing a rich framework for analysis. Furthermore, as the celebrated KAM theorem demonstrates, when a non-integrable perturbation is introduced, these quasi-periodic solutions continue to occupy extensive regions of the phase space, highlighting their importance in the study of dynamical behavior.

A quasi-periodic function is a map $\psi: \mathbb{R} \rightarrow \mathbb{R}^m$ that can be written as $\psi(t) = \Psi(t\omega_0 + \theta_0^0, \dots, t\omega_d + \theta_d^0)$ where $\Psi: \mathbb{T}^{d+1} \rightarrow \mathbb{R}^n$, $\Omega \stackrel{\text{def}}{=} (\omega_0, \dots, \omega_d)$ is called the frequency vector, and $(\theta_0^0, \dots, \theta_d^0)$ is the initial phase. Given a smooth vector field f defined for some open set of \mathbb{R}^m , a quasi-periodic trajectory to the flow given by f is a smooth quasi-periodic function that satisfies the following invariance equation:

$$\sum_{i=0}^d \frac{\partial \psi(\theta)}{\partial \theta_i} \omega_i = f(\psi(\theta)), \quad \theta = (t\omega_0 + \theta_0^0, \dots, t\omega_d + \theta_d^0). \quad (9)$$

If $\langle k, \Omega \rangle = 0$ for some $k \in \mathbb{Z}^{d+1}$, we say that Ω is resonant. The module

$$\mathcal{M}_\Omega = \{k \in \mathbb{Z}^{d+1} : \langle k, \Omega \rangle = 0\},$$

is called resonance module associated to the vector of frequencies Ω and it can be shown that it is a subgroup of \mathbb{Z}^{d+1} . When $\dim \mathcal{M}_\Omega = 0$, the vector Ω is said to be non-resonant and the trajectory ψ fills densely an invariant $(d+1)$ -torus i.e. $\mathbb{T}^{d+1} = \mathbb{R}^{d+1}/\mathbb{Z}^{d+1}$. For this reason, it is customary in the literature to refer to quasi-periodic solutions as invariant tori. More generally, if $\dim \mathcal{M}_\Omega = d+1-r$, the solution is dense in a r -dimensional torus and notice that in the extreme case, $\dim \mathcal{M}_\Omega = d$, the solution is, in fact periodic. This one is called completely resonant case.

When a quasi-periodic orbit is cut by a suitable section Σ , it becomes a quasi-periodic orbit of the associated Poincaré map P_Σ and its dimension (namely, the number of angles used to parameterise the solution) is reduced by one (see Figure 1). More precisely, the reduced invariant torus can be parameterised as $\varphi: \mathbb{T}^d \rightarrow \Sigma$ and satisfies the invariance equation

$$P_\Sigma \circ \varphi = \varphi \circ R_\omega,$$

where $R_\omega(s) = s + \omega$ is the fixed-rotation map of angle $\omega \in \mathbb{T}^d$.

Thus, the vector of frequencies ω of the sliced invariant torus is changed and depends on the section Σ . The goal of this section is to study how we can recover the frequencies of the original quasi-periodic function once we have computed its restriction to a Poincaré section¹.

To cope with this problem it is crucial that the torus is invariant by the flow. Thus, we can make this question solvable by considering the inner dynamics on the torus which we have assumed to be linear and quasi-periodic. Hence, the starting point of the discussion is a linear quasi-periodic flow on a torus, commonly called Kronecker flow.

Definition 16 (Kronecker flow). A Kronecker (linear quasi-periodic) flow on \mathbb{T}^{d+1} is a function

$$\begin{aligned} K_\Omega: \mathbb{T}^{d+1} \times \mathbb{R} &\rightarrow \mathbb{T}^{d+1} \\ (\theta, t) &\mapsto \theta + t\Omega. \end{aligned}$$

The vector $\Omega \in \mathbb{T}^{d+1}$ is called vector of frequencies. If $\langle k, \Omega \rangle \neq 0$ for all $k \in \mathbb{Z}^{d+1} \setminus \{0\}$, the flow is said to be non-resonant.

A Kronecker flow K_Ω is the explicit solution to the linear Ordinary Differential Equation written in angle variables $\dot{\theta} = \Omega$. In particular, $\{K_\Omega(\cdot, t) : t \in \mathbb{R}\}$ is a family of symplectic diffeomorphisms of the torus that form a group: $K_\Omega(\cdot, t_1 + t_2) = K_\Omega(\cdot, t_2) \circ K_\Omega(\cdot, t_1)$ and $K_\Omega(\theta, 0) = \theta$. Thus for a fixed t , the map $K_\Omega(\cdot, t)$ is, in fact, a rigid rotation of the torus by an angle Ω and, elementary, is a symplectic transformation.

In a general situation, a $(d+1)$ -torus is embedded in an ambient space \mathbb{R}^m and it is common to slice it using a section that is also defined in \mathbb{R}^m . Again, our point of view is intrinsic to the torus. In the following, we provide a few standard definitions stated intrinsically. First we note that a general section can be defined as the graph of torus function.

Definition 17 (Section). A section Σ of a torus \mathbb{T}^{d+1} is a subset defined by an equation

$$\Sigma = \{\theta \in \mathbb{T}^{d+1} : \sigma(\theta) = 0\},$$

where $\sigma: \mathbb{T}^{d+1} \rightarrow \mathbb{R}$ is a function. The section is said to be smooth if σ is smooth.

In this work, we are interested in suitable sections of tori. For a section to be suitable, it has to comply with a dynamical condition and a topological condition. The dynamical condition requires the section to be transversal to a given Kronecker flow on the torus, which is the standard hypothesis for a section to be a Poincaré section.

Definition 18 (Poincaré section on a Kronecker flow). A smooth section Σ is a Poincaré section of the Kronecker flow K_Ω if it is transversal, i.e.

$$\langle \nabla \sigma(\theta), \Omega \rangle \neq 0, \quad \text{for all } \theta \in \Sigma.$$

The topological condition asks the section to actually remove an angle of the torus. We call such a section, a natural one.

Definition 19 (Natural Section). A smooth section Σ of a $(d+1)$ -torus is said to be natural if Σ is diffeomorphic to \mathbb{T}^d .

Given a Poincaré section and an initial condition, a relevant quantity is the so-called *flight time*, i.e. the minimal positive time needed by a trajectory to reach the section. Notice that this can be defined for any initial condition, regardless of whether it is contained in the section or not. For an initial condition on the Poincaré section, the flight time is the minimal time to return to the section for first time, which is even a more relevant quantity for our purposes. In this situation, the flight time is called *return time*. We can, therefore build a map associating the flight time to each initial condition.

¹Notice that if the Poincaré map is given by a temporal section the answer is trivial.

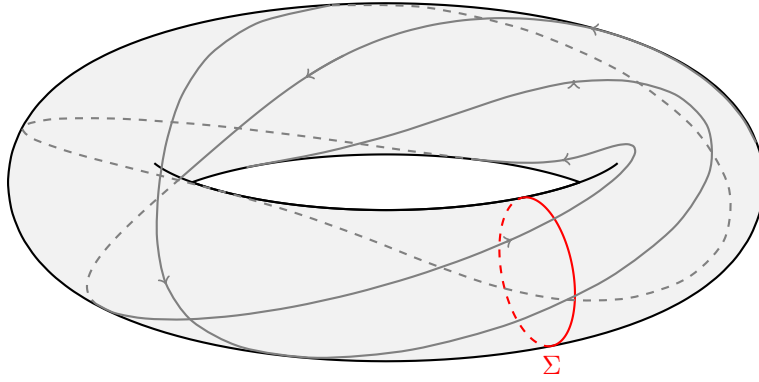


Figure 1: Representation of a Kronecker flow defined in a two-dimensional torus. A natural section Σ is depicted in red. See text for more details.

Definition 20 (Flight and return time maps). Given a Kronecker flow K_Ω and a Poincaré section Σ , the function

$$T_\Sigma: \mathbb{T}^{d+1} \rightarrow \mathbb{R}$$

$$\theta \mapsto \min_{T \in \mathbb{R}^+} \{K_\Omega(\theta, T) \in \Sigma\},$$

is called flight time map. The restriction of the flight time map to Σ is called the return time map.

The notion of Poincaré map itself can be stated intrinsically at this point.

Definition 21 (Poincaré map). Given a Poincaré section Σ and a Kronecker flow K_Ω on \mathbb{T}^{d+1} , we say that the map

$$P_\Sigma: \Sigma \rightarrow \Sigma$$

$$\theta \mapsto K_\Omega(\theta, T_\Sigma(\theta)),$$

is the Poincaré map related to Σ .

A natural section is defined by a topological property. Our computational approach, however, rely on parameterization of the section. There are, of course, infinitely many of them but we are interested on a parameterization that preserves the internal dynamics, i.e. one that makes the Poincaré map a rigid rotation of the d -torus. We call this kind of parameterization, compatible with the dynamics.

Definition 22 (Parameterization compatible with the dynamics). Let Σ be a natural Poincaré section. A parameterization $\varphi: \mathbb{T}^d \rightarrow \Sigma$ is said to be compatible with the dynamics if there exists $\omega \in \mathbb{T}^d$ such that

$$P_\Sigma(\varphi(s)) = \varphi(s + \omega), \quad \text{for all } s \in \mathbb{T}^d.$$

Lemma 23 (Existence of a parameterization compatible with the dynamics). *Given a quasi-periodic flow on a torus K_Ω and a natural Poincaré section, there always exists a parameterization compatible with the dynamics.*

Proof. We treat first the case $\Sigma_\ell = \{\theta_\ell \equiv 0 \pmod{1}\}$ for some ℓ between 0 and d . Let us consider the parameterization given by

$$\varphi_\ell: \mathbb{T}^d \rightarrow \Sigma_\ell$$

$$s = (s_0, s_2, \dots, s_{\ell-1}, s_\ell, \dots, s_d) \mapsto (s_0, s_2, \dots, s_{\ell-1}, 0, s_{\ell+1}, \dots, s_d).$$

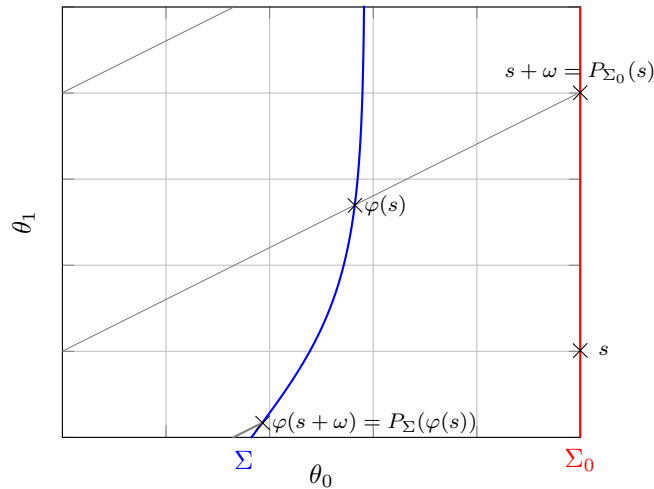


Figure 2: Construction of the homeomorphism that maps an arbitrary Poincaré section to a constant one. This is used in the proof of Lemma 23.

In this case the section is a straight line in the coordinates $(\theta_0, \theta_2, \dots, \theta_d)$. Moreover, the time return map is constant over Σ_ℓ . Indeed, it is determined by the equation $1 + \Omega_\ell T_{\Sigma_\ell} \equiv 2 \pmod{1}$, therefore

$$T_{\Sigma_\ell} = \frac{1}{\Omega_\ell}.$$

By construction,

$$P_{\Sigma_\ell}(\varphi_\ell(s)) = \varphi_\ell(s + \omega),$$

if $\omega = \varphi_\ell^{-1}(\Omega/T_{\Sigma_\ell})$.

Let us consider now a general section Σ . We can define a parameterization of this section by means of the following commutative diagram (see also Figure 2):

$$\begin{array}{ccc} \mathbb{T}^d & \xrightarrow{\varphi_\ell} & \Sigma_\ell \\ & \searrow \varphi & \downarrow K_\Omega(\varphi_\ell(s), T_\Sigma(\varphi_\ell(s))) \\ & & \Sigma \end{array}$$

Given $\tilde{\theta} \in \Sigma$, it can be written as $\tilde{\theta} = \varphi(s)$, for some $s \in \mathbb{T}^d$. Then:

$$\begin{aligned} P_\Sigma(\varphi(s)) &= K_\Omega(\varphi(s), T_\Sigma(\varphi(s))) \\ &= K_\Omega(\varphi(s), T_{\Sigma_\ell}(\varphi(s)) + T_\Sigma(s + \omega)) \\ &= K_\Omega(s + \omega, T_\Sigma(s + \omega)) = \varphi(s + \omega). \end{aligned}$$

Therefore, φ is a K_Ω -compatible parameterization. □

Theorem 24 (Invariance of the averaged return time). *Let K_Ω be Kronecker flow on \mathbb{T}^{d+1} , Σ a natural Poincaré section and T_Σ the flight time map, then*

$$\int_\Sigma T_\Sigma = \frac{1}{\Omega_\ell},$$

for some $\ell \in \{0, \dots, d\}$ depending on Σ .

Proof. The section Σ is natural and, therefore, by Lemma 23, there exists ℓ and a K_Ω -compatible parameterization φ homotopic to φ_ℓ . The result follows from the change of variables theorem and the fact that a Kronecker flow is volume preserving i.e. $\det D_\theta K_\Omega(\theta, t) = 1$ for all t . It follows that,

$$\int_\Sigma T_\Sigma = \int_{\Sigma_\ell} T_\Sigma \circ K_\Omega(\varphi_\ell(s), T_\Sigma(\varphi_\ell)) ds = \int_{\Sigma_\ell} T_{\Sigma_\ell} = \frac{1}{\Omega_\ell}. \quad \square$$

Remark 25. The average of the return-time does not depend on the Poincaré section as long as it is homotopic to $\{\theta_\ell \equiv 0 \pmod{1}\}$. This means that there are $(d + 1)$ -different averages for each torus.

Notice that the accuracy of the recovered frequency depends, essentially, on the accuracy of the frequencies computed on the Poincaré section and the return time map. At least, under quite general conditions of regularity on the return time map (which are guaranteed by the smoothness of the Poincaré section). Then, we can take advantage on the convergence properties of the trapezoidal rule to compute the integral in Theorem 24 (or equivalently to (19) later on).

Theorem 26 ([DB08]). *Suppose that the trapezoidal rule is applied with step-size h to integrate a function f over \mathbb{T} . Let us define the Fourier transform of f as*

$$\tilde{f}(\chi) = \int_{\mathbb{T}} f(s) \exp(-2\pi i \chi s) ds,$$

and $E(h)$ the integration error. Then,

$$E(h) \sim 2\tilde{f}(1/h).$$

This classic result states that the integration error of the trapezoidal rule applied to a periodic function behaves as its Fourier coefficients. In particular, if the function is a trigonometric polynomial, the integration error is zero provided that $h \leq 1/(2N + 1)$ where N is the degree of the polynomial. If the function is analytic, the integration error decreases exponentially with the integration step (this is called super-convergence). This results applies to the integral in Theorem 24 by using Fubini's Theorem in each integral coordinate.

4.1 Visualization of tori

In computer graphics, basic object visualization is achieved by creating a mesh of the object and connecting these mesh points with lines and faces. In our setting we have two possible objects to visualize: the full torus for the flow, \mathbb{T}^{d+1} , and a codimension 1 slice, \mathbb{T}^d , see Figure 1.

Let us assume that we have a Poincaré map P_Σ from a Poincaré section $\Sigma \subset \mathbb{T}^{d+1}$ and a Kronecker flow K_Ω on \mathbb{T}^{d+1} as in the Definition 21. A slice of \mathbb{T}^{d+1} compatible with the Kronecker dynamic is given by the graph of an invariant curve $\varphi: \mathbb{T}^d \rightarrow \Sigma$ that satisfies Definition 22 for an angle $\omega \in \mathbb{T}^d$. Thus, to visualize such a slice the dynamic of the torus is just to plot the graph of φ .

On the other hand, to visualise the torus \mathbb{T}^{d+1} only having as inputs P_Σ , φ , and ω may require deriving additional information. Indeed, the frequency vector Ω in \mathbb{T}^{d+1} may not be given explicitly in a generic setting such as when P_Σ is a flow coming from a spatial section of an ODE and the pair (φ, ω) has been obtained after imposing the invariance equation $P_\Sigma \circ \varphi = \varphi \circ R_\omega$. Then, in such a context, the frequency vector $\Omega \in \mathbb{T}^{d+1}$ is not known explicitly. Nevertheless, Theorem 24 indicates that we can obtain Ω and therefore we can visualize \mathbb{T}^{d+1} using φ , Ω , and the ODE-flow. In particular, the torus \mathbb{T}^{d+1} will be discretised by using φ and the flow. However, to show the lines and faces connecting nicely mesh points, we must untangle the Kronecker dynamics.

More precisely, assume, without loss of generality that after a possible diffeomorphism, Σ is homeomorphic to the natural section $\Sigma_0 = \{\theta \in \mathbb{T}^{d+1} : \theta_0 \equiv 0 \pmod{1}\}$. From Theorem 24 we get a number ω_0 and then the frequency vector $\Omega \in \mathbb{T}^{d+1}$ can be written in terms of the known $\omega \in \mathbb{T}^d$. The explicit

relation is $\Omega = \Omega_0(1, \omega)$. Now, the internal dynamics of \mathbb{T}^{d+1} is given by the Ω -Kronecker flow, hence, the mesh points will consist in evaluation of a map $\psi: \mathbb{T}^{d+1} \rightarrow \mathbb{T}^{d+1}$ of the form:

$$\psi(\theta_0 + t\Omega_0, \theta_2 + t\Omega_2, \dots, \theta_d + t\Omega_d)$$

for $(\theta_0, \theta_2, \dots, \theta_d) \in \mathbb{T}^{d+1}$. The map ψ parameterizes the \mathbb{T}^{d+1} and it can be obtained in terms of φ and P_Σ by isolating t . Indeed, if $(\theta_0^{j_1}, \theta_2^{j_2}, \dots, \theta_d^{j_d})$ is a mesh node, let $\tau \stackrel{\text{def}}{=} T_\Sigma(\theta_1^{j_2}, \dots, \theta_d^{j_d})$ be the flying time, then the mesh point will be

$$\psi(\theta_0^{j_1}, \dots, \theta_d^{j_d}) = \varphi(\theta_1^{j_2} + \theta_0^{j_1} \tau \Omega_1, \dots, \theta_d^{j_d} + \theta_0^{j_1} \tau \Omega_d) + \theta_0^{j_1} \tau. \quad (10)$$

The expression in (10) untangles the internal torus dynamics first by starting always from elements in Σ_0 , using the internal dynamics K_Ω , and by taking a point on the slice φ such that after $\theta_0^{j_1} \tau$ time, it lands in a point which is properly connected with the previous node.

5. Explicit torus construction on elliptic Hamiltonian points

Motivated by classical problems in Mechanical Systems, we present an application where high-order normal forms computed by Algorithm A, allow for the explicit derivation of invariant tori and characterization of the full frequency vectors. The framework we are about to present arises naturally in Hamiltonian systems or in systems with conserved quantities. A Poincaré map in these systems inherits specific properties, such as, energy conservation. Thus if a Poincaré map P described as a time-flow map after fixing an energy level and a spatial section has a fixed point z_0 , then the monodromy matrix inherits spectrum constraints due to the energy conservation. In particular, the product of the eigenvalues of such a matrix must be equal one.

The setting we present considers a fully elliptic fixed point z_0 , i.e., the eigenvalues of its monodromy matrix all lie on the unit circle. Then the procedure explicitly computes the changes of coordinates such that the original system is (locally) conjugated to an integrable system of the form

$$\begin{pmatrix} I \\ \theta \end{pmatrix} \mapsto \begin{pmatrix} I \\ \theta + \omega(I) \end{pmatrix}, \quad (11)$$

where (I, θ) are coordinates in a high-dimensional cylinder.

The orbits in (11) are all in invariant tori whose rotation vectors depend on the action I and they determine the dynamic in each of those objects. Maps like (11) are called *twist maps* and they are the equivalent to integrable Hamiltonian system.

The map $I \mapsto \omega(I)$ identifies an action I with its frequency vector $\omega(I)$. When such a map is invertible then, one is able to identify frequencies with actions. This invertibility is a necessary condition for the existence of tori in perturbed systems. By the inverse function theorem, the map $I \mapsto \omega(I)$ is (locally) invertible as long as $\det \omega'(I) \neq 0$. This condition is called *twist condition* and it appears in KAM theory. The construction process we present will be able to check the twist condition and quantify the existence of tori in nearby system.

Remark 27 (dimension). Notice that the described Poincaré map P is a $2n$ -dimensional system, however, the full phase space dimension will be $2n + 2$; one extra for fixing the energy level and a second one for fixing a spatial section.

5.1 Construction of high-dimensional twist maps

Let us consider an elliptic fixed point $z_0 \in \mathbb{R}^{2n}$ of a discrete dynamical system P , i.e. $P(z_0) = z_0$ and assume that the matrix $DP(z_0)$ has complex eigenvalues $\lambda_1, \bar{\lambda}_1, \dots, \lambda_n, \bar{\lambda}_n$ such that $\lambda_j \bar{\lambda}_j = 1$ for

$j = 1, \dots, n$. If we apply Algorithm A, then there will be unavoidable resonances due to the eigenvalue structure. Indeed, the resonance condition at order k is translated into

$$\lambda_i - \prod_{l=1}^n \lambda_l^{j_l} \lambda_l^{-j_{n+l}} = 0 \quad \text{or} \quad \lambda_i^{-1} - \prod_{l=1}^n \lambda_l^{j_l} \lambda_l^{-j_{n+l}} = 0. \quad (12)$$

for $j = (j_1, \dots, j_{2n}) \in \mathbb{N}^{2n}$, $|j| = k$, and $i = 1, \dots, n$. For clarity of exposition, we assume that all the eigenvalues are pairwise different. Then a resonance will occur whenever $j_l = j_{n+l}$ for all $l \neq i$ and $j_i - j_{n+i} = \pm 1$.

In such a case the normal form will consist in (p_i, q_i) for $i = 1, \dots, n$ of the form:

$$p_i(s_1, \dots, s_{2n}) = \lambda_i s_i + \sum_{k \geq 1} \sum_{\substack{|j|=k \\ j_l = j_{n+l}, \forall l \neq i \\ j_i - j_{n+i} = 1}} a_j s^j, \quad q_i(s_1, \dots, s_{2n}) = \bar{\lambda}_i s_{n+i} + \sum_{k \geq 1} \sum_{\substack{|j|=k \\ j_l = j_{n+l}, \forall l \neq i \\ j_i - j_{n+i} = -1}} b_j s^j, \quad (13)$$

whose monomial exponents coincide with a zero denominator in step 6a of the Algorithm A.

Equation (13) satisfies two relevant properties: *i*) both have the same number of monomials and *ii*) the eigen-decomposition gives conjugate eigenvectors, $b_j = \bar{a}_j$.

Remark 28 (about consistency requirement). The order $(p_1, \dots, p_n, q_1, \dots, q_n)$ and expressions in (13) are determined by step 3 of Algorithm A and, in particular, by its change $c_1(s)$. It is indeed possible to rearrange everything as long as it is consistent and it keeps track of all coordinate and symbols permutations. In the writing of (13) we have implicitly assumed that the diagonal eigenvalue matrix has entries ordered by $\lambda_1, \dots, \lambda_n, \bar{\lambda}_1, \dots, \bar{\lambda}_n$ and the eigenvector matrix has columns $v_1, \dots, v_n, \bar{v}_1, \dots, \bar{v}_n$, where v_i is eigenvector of eigenvalue λ_i for $i = 1, \dots, n$.

By assumption, the eigenvalues lie on the unit circle, i.e. $\lambda_i = e^{2\pi i \alpha_i}$ for $i = 1, \dots, n$. Therefore, the whole normal form (p_i, q_i) can be expressed by power series ω_i whose complex exponential recovers (p_i, q_i) . More precisely, let us consider complex symbols w_1, \dots, w_n such that $w_j \bar{w}_j = r_j^2$ with r_j a real symbol. Then we pick, for instance, p_i to compute ω_i

$$p_i(w_1, \dots, w_n, \bar{w}_1, \dots, \bar{w}_n) = e^{2\pi i \omega_i(r_1, \dots, r_n)} w_i, \quad i = 1, \dots, n. \quad (14)$$

Equivalently, one could have considered

$$q_i(w_1, \dots, w_n, \bar{w}_1, \dots, \bar{w}_n) = e^{-2\pi i \omega_i(r_1, \dots, r_n)} \bar{w}_i, \quad i = 1, \dots, n, \quad (15)$$

which means that ω_i is determined up to a sign.

The relation (14) shows an explicit way to compute ω_i via power series manipulation. More precisely, by isolating (logarithm and $2\pi i$ quotient) ω_i from

$$e^{2\pi i \omega_i(r_1, \dots, r_n)} = \frac{p_i(s_1, \dots, s_n, s_{n+1}, \dots, s_{2n})}{s_i} \Bigg|_{\substack{s_i = w_i \\ s_{n+i} = \bar{w}_i \\ w_i \bar{w}_i = r_i^2}}, \quad i = 1, \dots, n.$$

Similarly, one could have deduced how to get $-\omega_i$ from (15).

Proposition 29. *For all $i = 1, \dots, n$, the power series ω_i in (14) has real coefficients and it is of the form*

$$\omega_i(r) = \alpha_i + \sum_{k \geq 1} \sum_{|j|=k} \alpha_{i,2j} r^{2j},$$

with $r = (r_1, \dots, r_n)$. In particular, if p_i is truncated at order N , then ω_i is only known up to order $\lfloor \frac{N}{2} \rfloor$.

Proof. Let us prove by contradiction that $\alpha_{i,2j}$ are all real. If they have an imaginary part since r is a real vector symbols, then $\omega_i(r)$ would also have imaginary power series part and that would contradict its construction in (14). \square

5.1.1 Example: twist map in the plane

Equation (13) has explicit monomials that persist under the normal form process. These monomials have exponents that satisfy the resonance condition (12). As an example, when $n = 1$, (13) becomes

$$\begin{aligned} p_1(s_1, s_2) &= \lambda s_1 + a_{2,1} s_1^2 s_2 + a_{3,2} s_1^3 s_2^2 + O_6 \\ q_1(s_1, s_2) &= \bar{\lambda} s_2 + \bar{a}_{2,1} s_1 s_2^2 + \bar{a}_{3,2} s_1^2 s_2^3 + O_6 \end{aligned}$$

where O_6 stands for high order terms. Note that (13) contains extra crossing terms for $n \geq 2$.

The polynomial $Q(w) \stackrel{\text{def}}{=} p_1(w, \bar{w}) = \lambda w + a_{2,1} w^2 \bar{w} + a_{3,2} w^3 \bar{w}^2 + O_6$ allows to compute the corresponding twist map. Indeed, if $w \bar{w} = r^2$, then

$$\lambda w + a_{2,1} w^2 \bar{w} + a_{3,2} w^3 \bar{w}^2 = e^{2\pi i(\alpha_0 + \alpha_2 r^2 + \alpha_4 r^4)} w + O_6$$

where α_k are computed recurrently

$$l_{2k} = \frac{1}{\lambda} \left(a_{k+1,k} - \frac{1}{k} \sum_{j=1}^{k-1} j a_{k-j+1,k-j} l_{2j} \right), \quad \alpha_{2k} = \frac{l_{2k}}{2\pi i} \quad k \geq 1,$$

which comes from imposing the condition

$$\lambda \exp \left(2\pi i \sum_{k \geq 1} \alpha_{2k} r^{2k} \right) = \lambda + \sum_{k \geq 1} a_{k+1,k} r^{2k}.$$

5.2 Effective computation of invariant tori

The output of Algorithm A up to order N is the normal form with its changes of coordinates c_1, \dots, c_N . If $c \stackrel{\text{def}}{=} c_1 \circ \dots \circ c_N$, then we build an invariant tori of radii $r = (r_1, \dots, r_n)$ by

$$z(\theta_1, \dots, \theta_n) \stackrel{\text{def}}{=} z_0 + c(r_1 e^{2\pi i \theta_1}, \dots, r_n e^{2\pi i \theta_n}, r_1 e^{-2\pi i \theta_1}, \dots, r_n e^{-2\pi i \theta_n}), \quad (16)$$

which satisfies (up to an accuracy level)

$$G \circ z(\theta) = z(\theta + \omega(r)), \quad \text{for all } \theta \in \mathbb{T}^n, \quad (17)$$

where $\omega = (\omega_1, \dots, \omega_n)$ obtained by (14) and G is a local expansion of P at z_0 .

The radii r must be within the validity range of the computation accuracy. The conditions such an accuracy will also determine the error in the equality (17). There are different source of errors, such as the order N or the accuracy of the local approximation G . Note also that because a normal form is generically a semianalytical series, so is ω_i . These series have an asymptotic property but, in case of divergence, their validity range tends to zero instead of to a convergent radii.

Remark 30 (about signs). Note that one must be coherent with the signs of ω_i . That is, if one uses the ω_i from (15) or mixes between (14), then (16) must be changed accordingly in order to satisfy the invariance equation (17).

5.3 Tori construction from frequency recovery

The main conclusion of Theorem 24 is that all natural sections have the same averaged return time as long as they are homotopic on the torus (i.e. they eliminate the same angle). Moreover, the averaged return time on the section can be used to recover the frequencies of the original torus. Following the setting of the previous sections, the local expansion of P at the fixed point z_0 also provides the local expansion of the flying time. More precisely, if $P(x) = \Phi(T(x), x)$ where Φ is the baseline evolution process from the initial condition x to flying time $T(x)$ onto a Poincaré section, then the local expansion is a formal power

series expansion $G(s) = P(z_0 + s)$. In the procedure to obtain $G(s)$ we also get the power series $T(z_0 + s)$. Let $\mathcal{T}(s)$ be the formal power series defined by composition of the changes of coordinates c_1, \dots, c_N from Algorithm A, i.e.

$$\mathcal{T}(s) \stackrel{\text{def}}{=} T(z_0 + c_1 \circ \dots \circ c_N(s)). \quad (18)$$

Then Theorem 24 says that for $r = (r_1, \dots, r_n)$, the frequency $\omega_0(r)$ satisfies

$$\frac{1}{\omega_0(r)} = \int_{\mathbb{T}^n} \mathcal{T}(r_1 e^{2\pi i \theta_1}, \dots, r_n e^{2\pi i \theta_n}, r_1 e^{-2\pi i \theta_1}, \dots, r_n e^{-2\pi i \theta_n}) d\theta. \quad (19)$$

Thus the tori in the ODE phase space has frequency vector $\hat{\omega}(r) \stackrel{\text{def}}{=} \omega_0(r)(1, \omega_1(r), \dots, \omega_n(r))$. These tori can be visualized via a meshing process for each r , see Section 4.1. This process consists in evaluating a map $\psi: \mathbb{T}^{n+1} \rightarrow \mathbb{R}^{2n}$ in terms of its local parameterization $z(\theta)$, its evolution baseline process $\Phi(t, x)$, and frequency vector $\hat{\omega}$. More precisely,

$$\psi(\theta_0^{j_0}, \theta_1^{j_1}, \dots, \theta_n^{j_n}) = \Phi(\theta_0^{j_0} \tau, z(\theta_1^{j_1} + \theta_0^{j_0} \tau \omega_0 \omega_1, \dots, \theta_n^{j_n} + \theta_0^{j_0} \tau \omega_0 \omega_n)).$$

with $\tau = \mathcal{T}(r_1 e^{2\pi i \theta_1^{j_1}}, \dots, r_n e^{2\pi i \theta_n^{j_n}}, r_1 e^{-2\pi i \theta_1^{j_1}}, \dots, r_n e^{-2\pi i \theta_n^{j_n}})$.

Notice that in contrast to (10), we are using the actual flow from the ODE rather than the Kronecker flow in local torus coordinates.

Remark 31 (about the coherence requirement). As it was pointed in Remark 30, formula in (19) must be consistent with the computation choice of ω_i . Thus, (19) will provide the frequency for ω_i in (14). Moreover, r must be within the validity range of all the $\omega_i(r)$.

Remark 32 (preventing a numerical issue). From a numerical point of view, if the only goal is to compute (19), then one may omit and explicit computation of (18) to reduce the source of errors. Instead, one can compute the integral by trapezoidal rule's in a suitable mesh of $\theta \in \mathbb{T}^n$ with a good convergence rate, see Theorem 26.

6. Experiments

We use the public domain software `taylor` [GJZ22], which is an upgraded version of [JZ05]. The experiments were conducted on a standard laptop: an Intel i5 1.80GHz CPU with 4 cores, 8GB of RAM. Compilation was done using GNU C Compiler 12.2.0 with usual flags like `-O3`. The total runtime ranged from 2 to 3 minutes. The most resource-intensive tasks are *i*) computing the local initial approximation and *ii*) composition and reverse operation in Algorithm A. A minimally documented code sample is available². Due to the flexibility of [GJZ22], the code can easily be extended to arbitrary precision arithmetic, though it is not necessary for the current experiments.

We considered two experiments. The first involves the normal form, twist map, torus visualization of the Hénon-Heiles system expanding with respect to an energy level, see Section 6.1. The model is straightforward to describe and can be visualized easily. We have provided an thorough and detailed explanation, including a comparison of results across varying orders.

The second experiment also falls within the area of Mechanical Systems, where twist maps have traditionally been studied, see Section 6.2. The procedure largely mirrors that of the Hénon-Heiles experiment but extends to higher dimensions, so we have omitted repetitive details for clarity.

Both experiments are self-contained and do not require external datasets, aside from initial guesses of the dynamical objects that we already provide.

²<https://github.com/joang/nofo4maps>.

6.1 The Hénon-Heiles system

The Hénon-Heiles (HH) system is a Hamiltonian model proposed by Michel Hénon and Carl Heiles for the motion of a massless star under the attraction of an effective potential due to other stars in a galaxy [HH64]. The model is a two degrees of freedom Hamiltonian system with Hamiltonian

$$H = H(x, y, p_x, p_y) = \frac{1}{2}(p_x^2 + p_y^2) + \frac{1}{2}(x^2 + y^2) + x^2y - \frac{y^3}{3}. \quad (20)$$

The HH system stands out as a classical and simple example of chaotic conservative system. A common approach of investigation is through Poincaré maps. We will define such a map with elements on the section $\Sigma \stackrel{\text{def}}{=} \{x = 0\}$, with normal direction $\vec{n} = (1, 0, 0, 0)^\top$. The dynamics is described by a family of Area Preserving Maps (APM) parametrized by the energy (i.e. the Hamiltonian value).

We consider a discrete system given by the planar Poincaré map, P , obtained by using the spatial section Σ , the energy level $h_0 \stackrel{\text{def}}{=} 0.125$ (which determines p_x), and the flow associated with the Hamiltonian in (20). Thus, P first maps a value $z = (y, p_y)$ to $(x, y, p_x, p_y) \in \mathbb{R}^4$ with $x = 0$, and $p_x(h_0, x, z)$ determined by the Hamiltonian value h_0 . Then, it integrates the flow up to a time T determined after a second crossing with the section Σ and it returns to $\bar{z} = (\bar{y}, \bar{p}_y)$. The whole discrete system described by P can be summarised as

$$\bar{z} = P(T(z, h_0), z, h_0), \quad (21)$$

where $z = (y, p_y) \in \mathbb{R}^2$ and the return time T depends on z and the energy level h_0 .

Note that because p_x is determined by the energy level h_0 , not all $z \in \mathbb{R}^2$ is admissible. Therefore, the Poincaré map will be defined on a subset Ω on the plane. Note also that to discover the return time T , we must perform a root-finding method, such as a Newton method on the temporal variable.

6.1.1 Computation of a fixed point

We apply a Newton method to find a fixed point z_0 of the map P , i.e. $z_0 = P(T(z_0, h_0), z_0, h_0)$. The method requires to compute the derivative with respect to z which is related with the variational equations of the underlying ODE system given by the Hamiltonian (20). As the section Σ is spatial, the flight time is not constant. This requires to compute a projection of such a variational onto the section Σ (see [GJJC⁺23]). To perform the projection, we need to perform an infinitesimal correction of the variational flow around z_0 . Thus, we use a degree 1 jet with symbol s and compute $P(T(z + s), z + s)$ (we have temporarily removed the h_0 dependency in this section for clarity). Since the return time T depends on z , we have that $T(z + s) = T_0 + \tau_1 s$ where T_0 is the return time of the periodic orbit to the section Σ and τ_1 is the infinitesimal time correction. The value τ_1 is determined by imposing that the variational flow is in Σ . Once τ_1 is computed, we perform a temporal step with stepsize $\tau_1 s$, which will correct the variational flow and it will provide the final 2×2 matrix $D_z P(T(z), z)$ needed by the Newton method (and in the stability of the final periodic orbit z_0).

Figure 3 illustrates iterations of the Poincaré map P for different (y, p_y) values and common energy level h_0 as well as a periodic orbit on $\{p_y = 0\}$ with concrete values:

$$y_0 = 0.30266681746984 \quad \text{and} \quad T_0 = 6.07561578432290. \quad (22)$$

The periodic orbit given on (22) is elliptic and its linear stability is given by the monodromy matrix $D_z P(T(z_0), z_0)$. This matrix has the eigenvalues $e^{\pm 2\pi i \alpha}$ with $\alpha = 0.32460020136926$.

6.1.2 Computation of a curve of fixed points parametrized by the energy

The fixed point condition on the Poincaré map P depends on a parameter h_0 . This parameter is not explicit on the underlying ODE since it is given as a conserved quantity.

We want to demonstrate the power of jet transport by parametrizing the fixed point (z_0, T_0) given in (22) in terms of the energy level h_0 . Let us consider the function

$$F(z, h) \stackrel{\text{def}}{=} P(T(z, h), z, h) - z \tag{23}$$

and let us apply the Implicit Function Theorem to $F(z(h), h_0 + h) = 0$. The procedure, detailed in Section 2.3, requires that the monodromy matrix $D_z P(T(z_0, h_0), z_0, h_0)$ is invertible, which is indeed true.

The scheme involves the computation of high-order variational flows that each of them must be projected onto Σ to output a jet in 1 symbol in h . These derivatives with respect to the Hamiltonian value of the flow are obtained by using jet transport. Their projection onto the section Σ are done by computing the τ_k in the formal power series:

$$T(z_0 + h, h_0 + h) = T_0 + \sum_{k=1}^N \tau_k h^k. \tag{24}$$

Assume by induction that all the power series are truncated up to a degree, say m , and each of the τ_k have been computed recurrently. That is, assume we know τ_j for $j = 1, \dots, k-1$, τ_k consists in imposing that the k -th derivative of the flow is in Σ , which gives an explicit expression involving the normal direction \vec{n} of Σ , the tangent direction (i.e. the vector field evaluation) of the periodic orbit, and the k -th coefficient of the current jet. With the τ_k known, we correct the k -th derivative of the flow by applying a Horner's method on the temporal expansion of the vector field of the jet up to order m .

The computed m -th coefficient is precisely the one that we can now correct by solving the linear system with matrix $D_z F(z_0, h_0)$. Repeating sequentially this process with $k = 1, \dots, N$, we obtain the coefficients (in \mathbb{R}^2) of

$$z_0(h) = z_0 + z_1 h + \dots + z_N h^N. \tag{25}$$

As a by-product, we also obtain an expansion around the period T_0 that approximates the period of the different periodic orbits varying the energy level h , i.e. $T_0(h) \stackrel{\text{def}}{=} T(z_0(h), h_0 + h)$.

Note that, the fixed point curve is obtained using the same section Σ for all energy $h_0 + h$. This is a realistic condition because the coefficients in (25) are infinitesimal values around z_0 .

We use the validity range $h_{\max} \stackrel{\text{def}}{=} h_{\max}(10^{-16}, z_0(h))$ of the jet $z_0(h)$ of order N following (2). To compare the impact of the degree, we perform systematically a uniform scale, that is, $h \leftarrow h_* \sigma$ with $\sigma \in [-1, 1]$.

Figure 3 shows, for different degrees in h , the h_{\max} of the truncated power series of y and the period with the same tolerance $\epsilon = 10^{-16}$. Note that due to symmetries of the Hamiltonian (20), the curve $p_y(h)$ will be zero, meaning that the curve of fixed points will all lie in the axis $\{p_y = 0\}$. Since h_{\max} depends on the degree, the figure also shows the periodic curves and energy values reached up to the maximum degree considered.

6.1.3 Total power expansion at the fixed point curve

To apply the Algorithm A we first need to compute derivatives of the diffeomorphism P on the fixed point curve $z_0(h)$ with period curve $T_0(h)$. Note that if we were not performing the expansion on the energy around h_0 , then it would be enough to compute the derivatives on the data (z_0, T_0) , i.e. with $h = 0$.

Computing derivative of P with respect to the initial condition requires to compute high-order variational flows. In the HH model, it is achieved by using jet transport of a jet with 2 symbols (as many as coordinates of z) and a given degree D . The coefficients of these jets are other type of jets that encode the expansion with respect to the energy level, i.e. 1 symbol jet with another given degree N . Thus, what we want to compute is a nested jet:

$$G(h, s) \stackrel{\text{def}}{=} P(T(z_0(h) + s, h_0 + h), z_0(h) + s, h_0 + h). \tag{26}$$

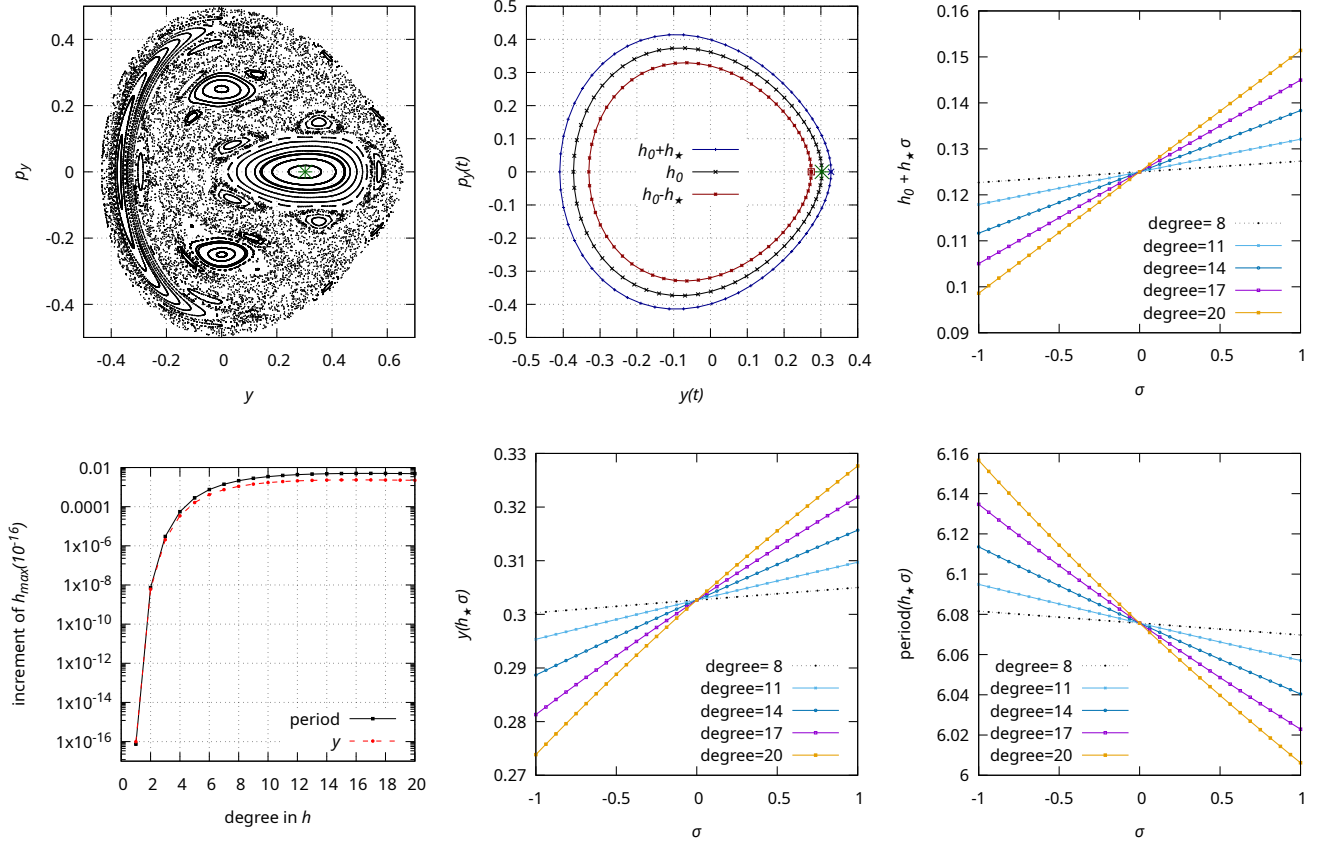


Figure 3: (1,1): Poincaré map (21) for the energy level $h_0 = 0.125$ and a fixed point with period T_0 in (22). (1,2): Periodic orbits for energies h_0 and $h_0 \pm h_*$ with $h_* = 0.02640858620272$ associated to a degree 20. (1,3): Values of the energy using different degrees. (2,1): Increment of the h_{\max} when using more degrees. (2,2-3): Values of y and period in terms of the degree in h .

The output is a jet in s with coefficients $z_j(h)$ for $|j| = 0, \dots, D$. Note that the number of coefficients needed in (26) is much smaller than using a jet with 3 symbols and degree $N + D$, due to simple combinatorial reasons as explained in Section 2.2.

Similarly as it happened when computing $z_0(h)$, the derivatives of the variational flow must be projected onto the uniform energy section Σ . This is achieved by finding $\tau_j(h)$ in the power expansion

$$\mathcal{T}(h, s) \stackrel{\text{def}}{=} T(z_0(h) + s, h_0 + h) = T_0(h) + \sum_{|j|=1}^D \tau_j(h) s^j. \quad (27)$$

Notice that because the data structures are nested jets, also the zero term in (27) needs to be projected to the section as well since only the zero coefficient in $T_0(h)$ is the flying time to section for the orbit. Thus, before finding any $\tau_j(h)$ we must first apply the initial correction given by $T_0(h)$. That is, to apply a Horner's method of the time-expanded vector field at the current jet and up to order $\max\{N, D\}$. Then the condition for $\tau_j(h)$ as homogeneous polynomial of order $|j|$ is the same as the one used in (24) with the difference that now we need the value of the vector field as a polynomial in h . All these jet manipulations are provided by the software [GJZ22].

Repeating sequentially the process for $|j| = 0$ up to D , we obtain the projected jet of jets $G(h, s)$ on the section and period expansion $\mathcal{T}(h, s)$. These jets have a total of $\binom{2+D}{2} \binom{1+N}{1}$ real numbers for each coordinate. In this section we have used $(N, D) = (20, 20)$ for the first Figures 3-4, and $(N, D) = (14, 5)$ for Figures 5-6.

Since the coefficient $|j| = 1$ provides the energy expanded monodromy matrix of the periodic orbit z_0 at energy h_0 , we can compute the energy dependent eigenvalues. In the HH case, it can be done by a direct planar eigenvalue formula or by the described method in Section 2.4. We check that the imaginary part is never zero on the safe validity interval $[-h_\star, h_\star]$. Thus, the curve of fixed points $z_0(h)$ are all elliptic in that energy interval. Figure 4 shows the validity range increment and the argument $\alpha_0(h)$ of the eigenvalues $\lambda(h) = e^{\pm 2\pi i \alpha_0(h)}$ of the elliptic fixed curve $z_0(h)$ for different degrees in h .

6.1.4 Normal form and twist map around the fixed point curve

The jet of jets $G(h, s)$ in (26) serves as input of the Algorithm A to output another nested jet $p(h, s)$ (in complex arithmetic) that encodes a normal form and a change of coordinates $c(h, s)$ around the fixed point curve $z_0(h)$. The step 6a in the algorithm determines possible obstructions due to resonances. In the case of HH, which is conservative, the a-priori resonance conditions translate into:

$$\lambda(h) - \lambda(h)^{j_1} \lambda(h)^{-j_2} = 0 \quad \text{or} \quad \lambda(h)^{-1} - \lambda(h)^{j_1} \lambda(h)^{-j_2} = 0, \quad (28)$$

for some $(j_1, j_2) \in \mathbb{N}^2$ and $\lambda(h)$ being the energy dependent eigenvalue. The combinations $j_1 - j_2 = \pm 1$ are unavoidable resonances satisfying (28). Thus, in absence of other resonances, the normal form $p(h, s)$ with components p_1 and p_2 will look like

$$\begin{aligned} p_1(h, s) &= \lambda(h)s_1 + p_{2,1}(h)s_1^2s_2 + p_{3,1}(h)s_1^3s_2^2 + \dots \\ p_2(h, s) &= \lambda(h)^{-1}s_2 + \overline{p_{2,1}(h)}s_1s_2^2 + \overline{p_{3,1}(h)}s_1^2s_2^3 + \dots \end{aligned} \quad (29)$$

where the wide bar denotes the coefficient-wise complex conjugate and $s = (s_1, s_2)$.

Note that if there was an \tilde{h} in the validity range of $\lambda(h)$ that satisfied a resonance condition (28), then we would still have a normal form like in (29) as long as the validity range for h was shrunk to be up to the smallest \tilde{h} on resonance. Through a non-rigorous numerical check, in our case of study, we do not need to shrink the validity range in h . The check amounts to numerically computing the quantities

$$\min_{\sigma \in [-1, 1]} |\mathcal{R}(h_\star \sigma)|$$

where $h_\star \stackrel{\text{def}}{=} 0.95h_{\max}(10^{-16}; \mathcal{R})$ is a safe validity range of the jet $\mathcal{R}(h)$ in each of the LHS of (28). The results of these computations are far from zero in different thinner σ meshes in $[-1, 1]$.

Once the normal form (29) has been computed, we construct the twist map as described in Section 5.1 by symbolically taking a complex number w such that $w\bar{w} = r^2$ and using one of the two jets of jets in $p(h, s)$, e.g. p_1 , we arrive to an integrable system parametrized by the energy $h_0 + h$

$$\begin{pmatrix} \theta \\ r \end{pmatrix} \mapsto \begin{pmatrix} r \\ \theta + \omega(h, r) \end{pmatrix} \quad \text{with} \quad \omega(h, r) = \alpha_0(h) + \sum_{k=1}^{D-1} \alpha_{2k}(h)r^{2k}. \quad (30)$$

The jet of jets $\omega(h, r)$ satisfies the relation described in Section 5.1, namely

$$e^{2\pi i \omega(h, r)} = \frac{p_1(h, s)}{s_1} \Big|_{\substack{s=(s_1, s_2)=(w, \bar{w}) \\ w\bar{w}=r^2}}.$$

This relation shows the way to compute $\omega(h, r)$ by applying the logarithm (of jets) and dividing by the imaginary number $2\pi i$. Note that if we were used p_2 instead of p_1 , we would have obtained an equivalent twist map but with $-\omega(h, r)$.

Remark 33 (numerical observation). Theoretically $\alpha_{2k}(0)$ in (30) are reals. Numerically, these numbers will have (small) imaginary part. Due to round-off propagation these imaginary parts cannot be neglected when evaluating $\omega(h, r)$. The size of these imaginary parts can vary from using the scaling factor in the normal form computation, see Remark 10.

Figure 4 shows the $\alpha_0(h)$ and $\alpha_2(h)$ validity ranges and their range value therein. Clearly $\alpha_2(h)$ is far from zero which implies the existence of perturbed tori.

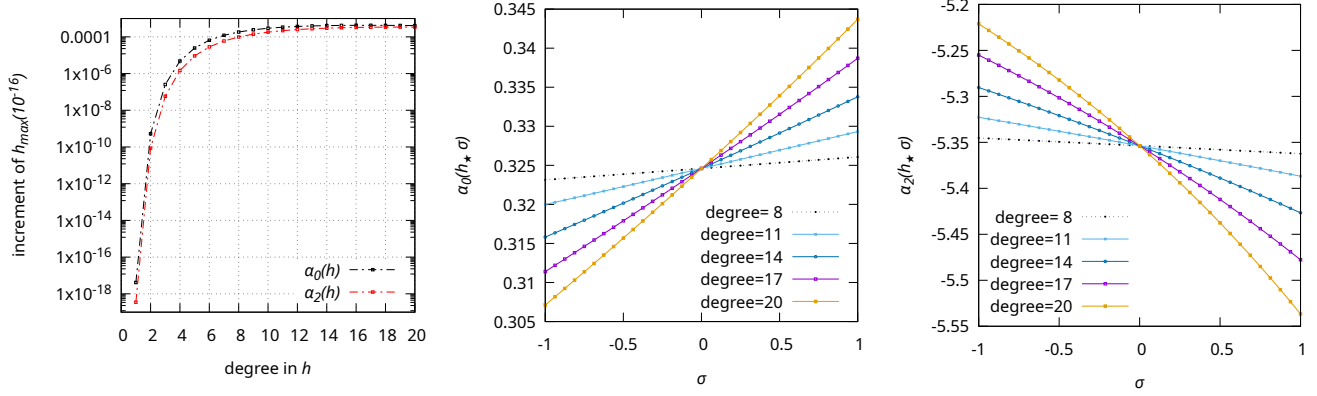


Figure 4: Increment validity ranges of $\alpha_0(h)$ and $\alpha_2(h)$ of the twist construction (30) and its values varying the energy level.

6.1.5 Invariant curve and torus frequencies

The twist map in (30) provides an explicit torus construction for the original HH system around the fixed elliptic point curve around z_0 and energy level h_0 , (22). Indeed, Algorithm A also provides the change of coordinates $c(h, s)$ from normal form coordinates to the original system. This change is given by composition of the polynomials in s , i.e. $c = c_1 \circ \dots \circ c_N$ (where the composition here refers to the variable s only).

We build the invariant curve $z_{h,r}: \mathbb{T} \rightarrow \mathbb{R}^2$ of the HH system by computing

$$z_{h,r}(\theta) \stackrel{\text{def}}{=} z_0(h) + c(h, re^{2\pi i\theta}, re^{-2\pi i\theta}), \quad (31)$$

where $z_0(h)$ is given in (25). These invariant curves parametrized by h and r satisfy an invariant equation, that is More precisely, for all h and r in their validity ranges,

$$G(h, z_{h,r}(\theta)) = z_{h,r}(\theta + \omega(h, r)), \quad \text{for all } \theta \in \mathbb{T}, \quad (32)$$

with $G(h, s)$ given in (26). The equation (32) is invariant in the sense that for all θ , the image by G (or P), it results in another element in the curve that has been shifted by $\omega(h, r)$ from the original one.

The invariant curve (31) is an embedding of 2-dimensional invariant object $\mathcal{K}_{h,r}$ homeomorphic to \mathbb{T}^2 . If we parametrize by a map $K_{h,r}: \mathbb{T}^2 \rightarrow \mathbb{R}^4$, there is a frequency vector $(\omega_1(h, r), \omega_2(h, r))$ such that

$$\mathcal{K}_{h,r} = \{K_{h,r}(\theta_1 + t\omega_1(h, r), \theta_2 + t\omega_2(h, r)): (\theta_1, \theta_2) \in \mathbb{T}^2 \text{ and } t \in \mathbb{R}\}, \quad (33)$$

is diffeomorphic to \mathbb{T}^2 . Theorem 24 tells us how to compute the frequency vector. First we compute $\omega_1(h, r)$ as the inverse of the quantity

$$T_1(h, r) \stackrel{\text{def}}{=} \int_0^1 \mathcal{T}(h_0 + h, c(h, re^{2\pi i\theta}, re^{-2\pi i\theta})) d\theta, \quad (34)$$

where $\mathcal{T}(h, s)$ is given in (27). Note that to obtain (34), we must compute

$$\mathcal{T}(h_0 + h, c(h, s)) = T_0(h) + \sum_{k \geq 1} \sum_{\substack{i+j=k \\ i, j \in \mathbb{N}}} a_{i,j}(h) s_1^i s_2^j,$$

we substitute $s = (re^{2\pi i\theta}, re^{-2\pi i\theta})$, and we finally use the linear properties of the integral to deduce

$$T_1(h, r) = T_0(h) + \sum_{k \geq 1} a_{2k, 2k}(h) r^{2k},$$

which similarly to Proposition 29 we can deduce that $a_{2k, 2k}(h)$ are real numbers.

Once we have $\omega_1(h, r)$, we then have $\omega_2(h, r) = \omega_1(h, r)\omega(h, r)$.

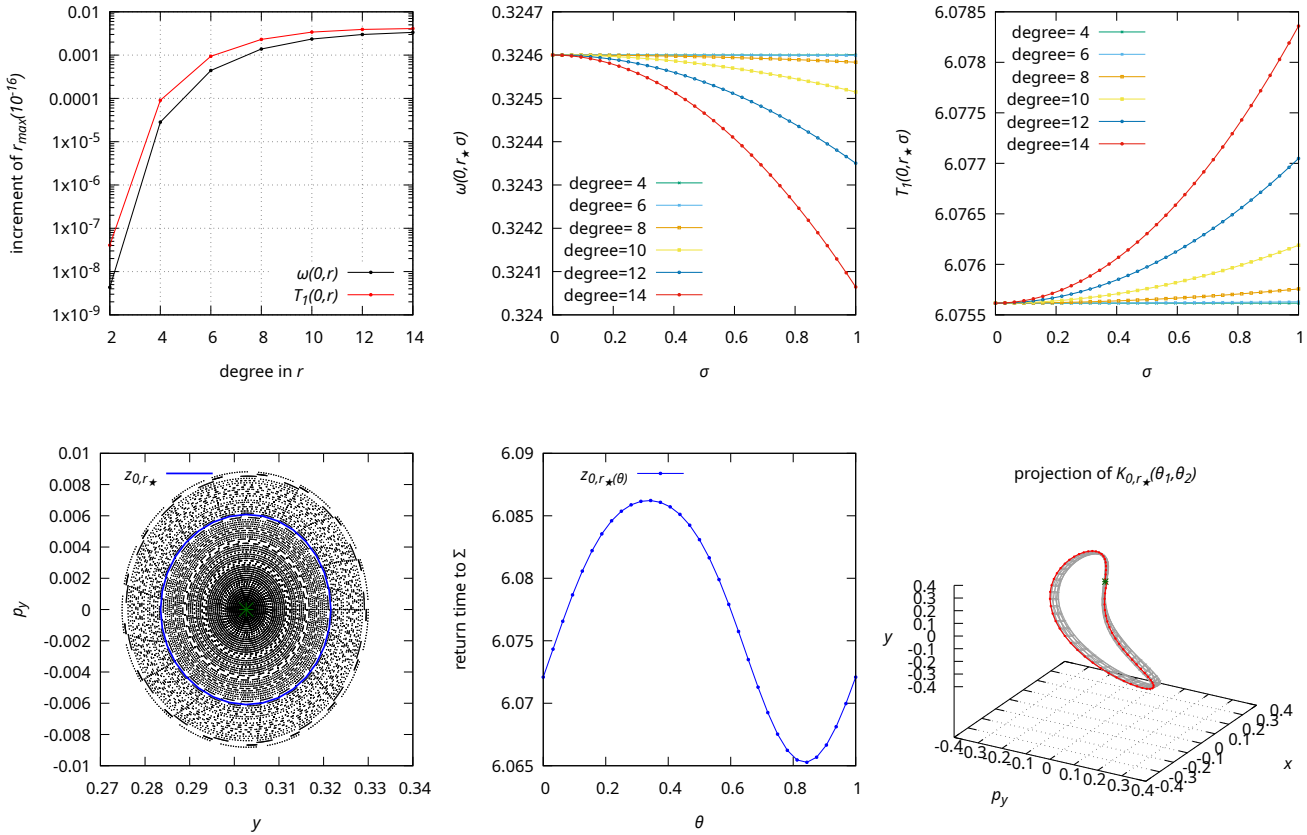


Figure 5: (1,1): Increment of validity ranges with respect to the radius r . (1,2-3): Values of $\omega(0, r)$ and $T_1(0, r)$ using different degrees in r . (2,1): Invariant curve using $r_* = 0.0100188767417$ of degree 14. (2,2): Return time of each of the of the invariant curve. (2,3): Invariant tori (grey), flow of the point with $\theta = 0$ in the invariant curve (red), fixed point (green) for an $\omega(0, r_*) = 0.32406438163539$.

6.1.6 Full torus visualization

A graphic visualization of the tori associated to an invariant curves is possible if one knows the invariant curve $z_{h,r}(\theta)$ and the frequency vector $\omega(h, r)$ in (32). We compute a table of values $K_{h,r}(\theta_1, \theta_2)$ in a suitable mesh of angles θ_1 and θ_2 . This mesh must be rectangles on the associated surface, for graphic visualization we must disregard the internal torus dynamics and adjust the table of values on the vertices of these rectangles. By knowing the internal dynamics of the torus, we can perform such rectangle connections, as it has been described in Sections 4.1 and 5.3.

Last panel in Figure 5 show a 3D torus versions with an integration of a point while Figure 6 shows its coordinate projection.

6.2 The Restricted Three Body Problem

The Restricted Three Body Problem (RTBP) is a model conceived to describe the motion of a test particle under the gravitational influence of two massive bodies (the so-called primaries). The primaries are assumed to move along a solution of the two body problem, typically, in circles along its common centre of mass. A classical textbook is [Sze67]. Formally speaking, the RTBP is a Hamiltonian system with three degrees of freedom, that, in suitable units and frame of reference reads as:

$$H = H(x, y, z, p_x, p_y, p_z) = \frac{1}{2}(p_x^2 + p_y^2 + p_z^2) + yp_x - xp_y - \frac{1-\mu}{r_1} - \frac{\mu}{r_2}, \quad (35)$$

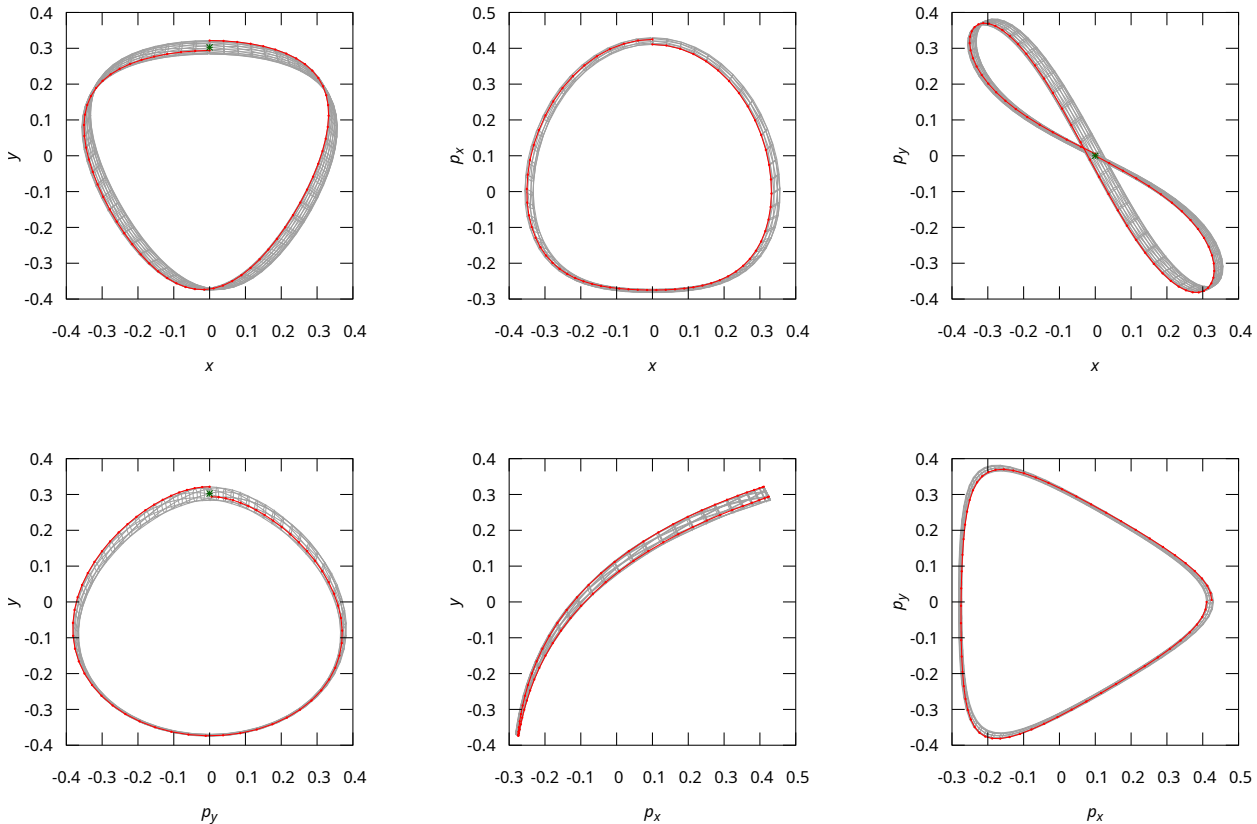


Figure 6: Coordinate projections of the torus in Figure 5.

where $\mu \leq 1/2$ is the mass in dimensional units of the smaller primary, $r_1^2 = (x - \mu)^2 + y^2 + z^2$ is the squared distance of the test particle to the larger primary, $r_2^2 = (x - \mu + 1)^2 + y^2 + z^2$ is the squared distance to the smaller primary and $p_x = \dot{x} - y$, $p_y = \dot{y} + x$, $p_z = \dot{z}$ are the momenta.

It is common knowledge that the RTBP has five equilibrium points L_i , $i = 1, \dots, 5$, named the Lagrangian Points. The collinear points (L_1 , L_2 and L_3) were discovered by Euler and are linearly unstable. On the other hand, the equilateral points (L_4 and L_5) are linearly stable if $\mu < \mu_R$. Here,

$$\mu_R \stackrel{\text{def}}{=} \frac{1}{2} \left(1 - \sqrt{23/27} \right) \approx 0.0385208965,$$

is the so-called Routh critical value. For $\mu > \mu_R$, the equilateral points are of complex-saddle type and, therefore, linearly unstable.

The stability of the equilateral points has awakened the interest of researchers since the discovery of the Trojan asteroids. Nonlinear behaviour near the Lagrangian points is a more involved issue. The Lyapunov centre theorem (see, for instance [AP95]) states that there is a family of periodic orbits that emanate from each eigenspace related to an elliptic (i.e. purely imaginary) eigenvalue.

Long term stability of trajectories near the equilateral points is provided by KAM theory in the case of two degrees of freedom (that is, if only the invariant subspace $\{z = 0, p_z = 0\}$ is considered). The case of three degrees of freedom is more involved due to the existence of Arnold diffusion, i.e. a process of diffusion driven by secondary unstable periodic orbits. This kind of instability, although generic is slow and consequently, the system behaves as a stable one for long time spans. These time spans can be estimated and the diffusion bounded by means of normal form techniques. In this example, we explore the neighbourhood of the equilateral L_4 for $\mu = 0.04$. Notice that this mass ratio is above Routh value, hence

L_4 is not linearly stable. The normal linear behaviour within the invariant subspace $\{z = 0, p_z = 0\}$ is of complex-saddle type. However, the orthogonal eigenspace has elliptic character and by the Lyapunov Theorem, it emanates a family of periodic orbits. Due to the fact that the family is locally (near L_4) orthogonal to the subspace $\{z = 0, p_z = 0\}$, this family is usually called vertical family of Lyapunov orbits. Close enough to L_4 , the family inherits the linear character of the equilibrium it raises from. However, at sufficient distance from $\{z = 0\}$, the family is totally elliptic and therefore practical stability is to be expected nearby.

6.2.1 Elliptic fixed point

We have selected a periodic orbit that is already analysed in [JV98] where a normal form based approach is employed to bound Arnold diffusion of long time spans. This periodic orbit is a periodic orbit of the vertical Lyapunov family characterised by a value of approximately $p_z = 0.25$ (which is equivalent to fix a certain value of the Hamiltonian (35)).

The coordinates of the periodic orbits (as a fixed point of the Poincaré map related to the section $\Sigma = \{z = 0, p_z > 0\}$) are given in Table 1, left column. The right column of 1 contains additional information: The first two rows provide the period of the orbit (T_0) and the value of the hamiltonian (H_0). By means of equation (35) and fixing H_0 , one can recover the value of p_z . The third and fourth row of the right column in Table 1 contain information about the linear normal behaviour related to the orbit as a fixed point of the Poincaré map. That is, the eigenvalues of the Jacobian matrix of the map are given by $\lambda_1^\pm = e^{\pm 2\pi i \alpha_1}$ and $\lambda_2^\pm = e^{\pm 2\pi i \alpha_2}$. The arguments of these eigenvalues, α_1 and α_2 , are the values provided by Table 1. These values indicate, at linear order, the frequencies of the families of invariant curves emanating from the fixed point which are tangent the eigendirections (see [JV97]). These values are usually called normal frequencies of the fixed point.

We have applied the algorithms explained in previous sections of the present paper to this periodic orbit. However, let us stress that, in [JV98], the approach is based on the Lie transformation method generalized to handle Taylor-Fourier series. Transforming the Hamiltonian function is, in fact, a standard method used in other works where normal forms about periodic orbits are computed, see [GJMS93, And02, GJ01, JJCR20, RJJC21a, RJJC21b, RJJC23]. As a side comment, all these mentioned works consider normal forms in periodic-time dependent Hamiltonian systems (namely, periodic perturbations of the restricted three body problem). The autonomous case tackled and in [JV98] is more involved as the Floquet Change of variables necessary to arrange the second order of the Hamiltonian demands extra care (again, see details in [JV98]). As we work directly on the Poincaré map, we do not need to cope with the Floquet Change.

x	-4.669907803550578e-01	T_0	6.286004008046577e+00
y	8.616112997374480e-01	H_0	-1.449088268767175e+00
p_x	-8.347975347250995e-01	α_1	2.531623016040890e-01
p_y	-4.524543662846999e-01	α_2	3.314789011607125e-01

Table 1: Coordinates of the fixed point in the Poincaré section Σ with Hamiltonian H_0 , period T_0 , and normal frequencies α_1 and α_2 . See text for more details.

6.2.2 Normal form and twist construction

We have implemented the methodology explained in the previous sections to compute a 4-dimensional twist map associated to the Poincaré map at the specific energy level H_0 in Table 1. In particular, and as opposed to Section 6.1, in the present case, the Poincaré map has not been expanded with respect to the energy level.

The first step to apply Algorithm A, consists on computing the Taylor polynomial of the Poincaré at the fixed point of Table 1. As an example, the expansion up to order 11 and 4 symbols takes about 45 seconds of CPU time.

After that, Algorithm A runs in around 3.2 minutes since in the neighbourhood provided by the high-order Poincaré derivatives only avoidable resonances are present. Hence, the algorithm's provides changes of coordinates and four truncated power series of the form (13), we have used as scaling factor $\varrho = 5.788752759731585\text{e-}03$. Then we solve (14), using jets of 2 symbols, to obtain $\omega_1(r_1, r_2)$ and $\omega_2(r_1, r_2)$ in Proposition 29.

Adding up, two-dimensional twist coordinates can be computed in 0.7 seconds in a neighbourhood of the periodic orbit in Table 1. The twist map condition given by the determinant of the following matrix

$$\begin{pmatrix} \frac{\partial^2 \omega_1}{\partial r_1^2}(0,0) & \frac{\partial^2 \omega_1}{\partial r_2^2}(0,0) \\ \frac{\partial^2 \omega_2}{\partial r_1^2}(0,0) & \frac{\partial^2 \omega_2}{\partial r_2^2}(0,0) \end{pmatrix} = \frac{1}{(2\pi\varrho)^2} \begin{pmatrix} -4.136303897444691\text{e-}04 & -9.728663974782056\text{e-}04 \\ 1.067616548567459\text{e-}03 & 1.155469385927883\text{e-}03 \end{pmatrix}.$$

If the determinant is different from zero, twist theorem ensures the persistence of two-dimensional KAM tori in the Poincaré section. Notice that these tori are three-dimensional in the original flow.

Table 2 shows the coefficients of the twist ω_1 and ω_2 at degree 10. Note that all the monomials are power 2 because of the radius, which means that the effective degree is 5. According to Proposition 29 the imaginary part of these coefficients are all real. In practice if the normal form is not scaled by the scaling factor ϱ , some of these imaginary part can numerically be far from machine precision.

$2\pi\omega_1(r_1, r_2)$	$2\pi\omega_2(r_2, r_2)$	k_1	k_2
1.590665653770496e+00	2.082743361413116e+00	0	0
-4.136303897444691e-04	1.067616548567459e-03	2	0
-9.728663974782056e-04	1.155469385927883e-03	0	2
1.239784629654938e-06	-3.469582163280214e-06	4	0
7.461178082695058e-06	4.782396906736634e-05	2	2
1.435493977600822e-05	3.999811918947041e-05	0	4
-4.893940486298444e-09	1.655876677634510e-08	6	0
-1.292392321865263e-07	5.015554940815004e-06	4	2
-4.379452993341237e-06	1.561084997403964e-05	2	4
-4.282160824526974e-06	9.558121027085274e-06	0	6
5.466632652962671e-12	-4.803565938164035e-11	8	0
1.378767712290349e-09	4.400815440393997e-07	6	2
-4.659485001412326e-07	2.440400198268105e-06	4	4
-1.062580313218477e-06	3.659445392752820e-06	2	6
-5.662648052671416e-07	1.623507030996212e-06	0	8
1.407435407399248e-13	-1.189493967595100e-13	10	0
-6.179070785891979e-12	3.898101773945702e-08	8	2
-7.158869553581880e-08	3.554868055453147e-07	6	4
-2.982243507624324e-07	9.711485715284952e-07	4	6
-3.648117449889493e-07	1.000066965663802e-06	2	8
-1.420755214098244e-07	3.514612623405018e-07	0	10

Table 2: Coefficients of $2\pi\omega_i(r_1, r_2) = \sum_{k_1, k_2} \alpha_{k_1, k_2}^i r_1^{k_1} r_2^{k_2}$ in its power expansion of r_1 and r_2 for $i = 1, 2$.

Figure 7 shows validity ranges, r_{\max} with tolerance $\epsilon = 10^{-16}$, and it uses a r_\star (see the value in the caption) what is the 0.95 times the minimum of the r_{\max} of ω_1 and ω_2 . Note that r_\star lies in the unit scaling of ϱ from which the normal form was computed.

Using the period expansion $T(s)$ and the changes of coordinates $c_1 \circ \dots \circ c_N$ of Algorithm A we compute the $\omega_0(r_1, r_2)$ as the integral in Theorem 24 and plotted in Figure 7. The computation of ω_0 uses a mesh

of 32×32 for (θ_1, θ_2) for each $(r_\star \sigma_1, r_\star \sigma_2)$, which meshes (σ_1, σ_2) in a same equispaced 32×32 mesh of $[0, 1]^2$ to compute the integral. The overall computational time to mesh ω_0 takes around 56 minutes. Note that in the mesh of (σ_1, σ_2) can easily be parallelized and the bottleneck here is mostly for a plotting purpose.

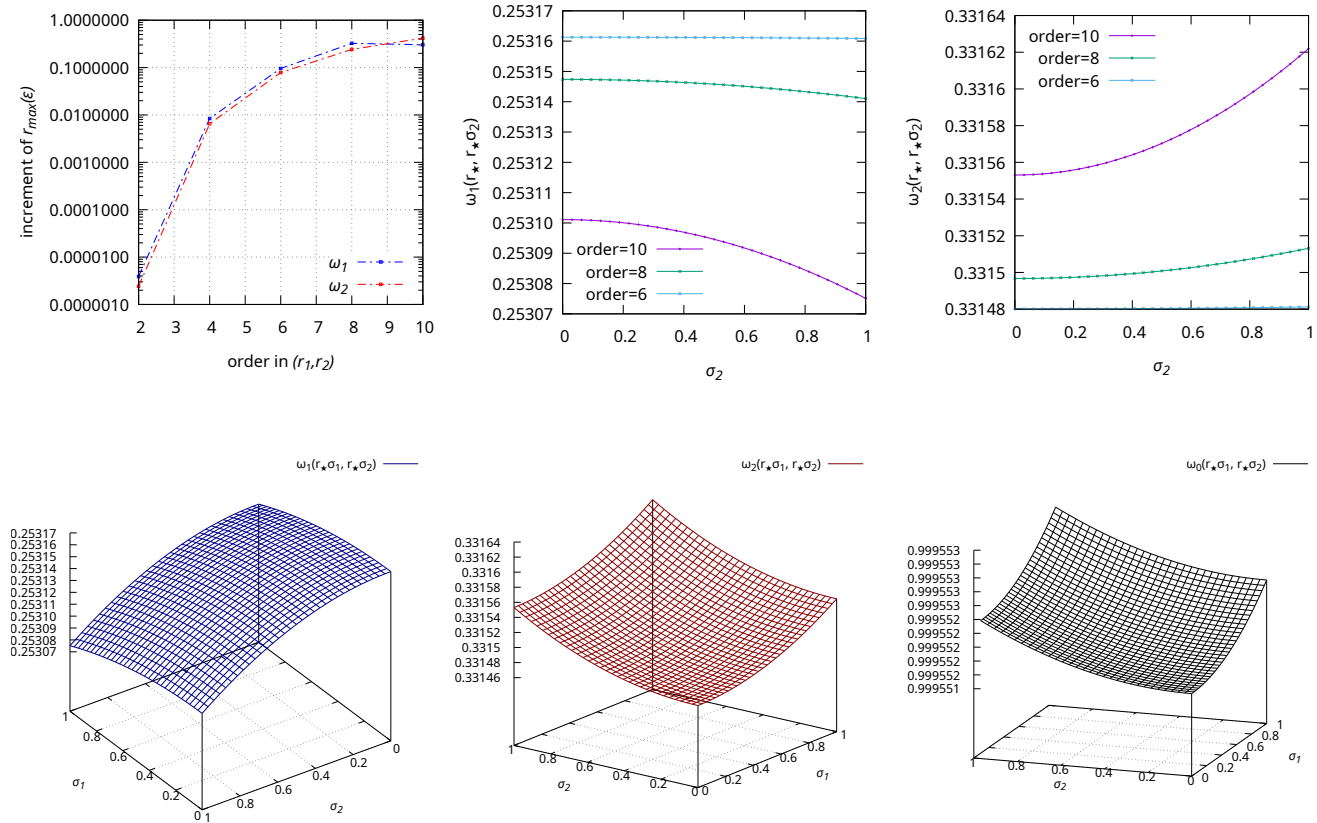


Figure 7: (1,1): Increment of validity ranges with tolerance $\epsilon = 10^{-16}$. (1,2-3): values of $\omega_j(r_\star, r_\star \sigma_2)$, $j \in \{1, 2\}$. (1-3,2): surfaces of $\omega_j(r_\star \sigma_1, r_\star \sigma_2)$, $j \in \{0, 1, 2\}$. Here $r_\star = 6.303157471364387\text{e-}01$.

6.2.3 Torus visualizations

Fixed the r_\star as in Figure 7's caption, we compute the intrinsic frequency vector

$$\omega_1(r_\star, r_\star) = 2.530751124713419\text{e-}01 \quad \text{and} \quad \omega_2(r_\star, r_\star) = 3.316219283594150\text{e-}01.$$

Using the changes of coordinate $c_0 \circ c_1 \circ \dots \circ c_N$ from the Algorithm A with $N = 11$, we obtain, in just 2 seconds, torus parametrizations of $(x, y, p_x, p_y): \mathbb{T}^2 \rightarrow \mathbb{R}^4$ in a neighbourhood of the fixed Poincaré point in Table 1. For each of these points we can compute the flying time T_Σ to the section by a direct integration (we could have used the expansion T too). Figure 8 shows these 2-D torus using a 32×32 equispaced mesh of (θ_1, θ_2) . In particular, we have added in red (scaled by 0.002) the unit vectors corresponding to (p_x, p_y) .

Moreover, by using the $\omega_0(r_\star, r_\star) = 9.999532699061624\text{e-}01$, and the flow from the ODE Hamiltonian (35), we can visualize the 3-D torus as described in Section 5.3. In this case, Figure 9 shows first some slices of θ_0 all with the red scaled unit vector of (p_x, p_y, p_z) except for the ones starting at the section Σ . We have also plotted the integration of two points on Σ which corresponds to an orbit that reaches the initial torus with a shift (ω_1, ω_2) . The other two are just the straightforward 3-D tori plots of (x, y, z) and (p_x, p_y, p_z) .

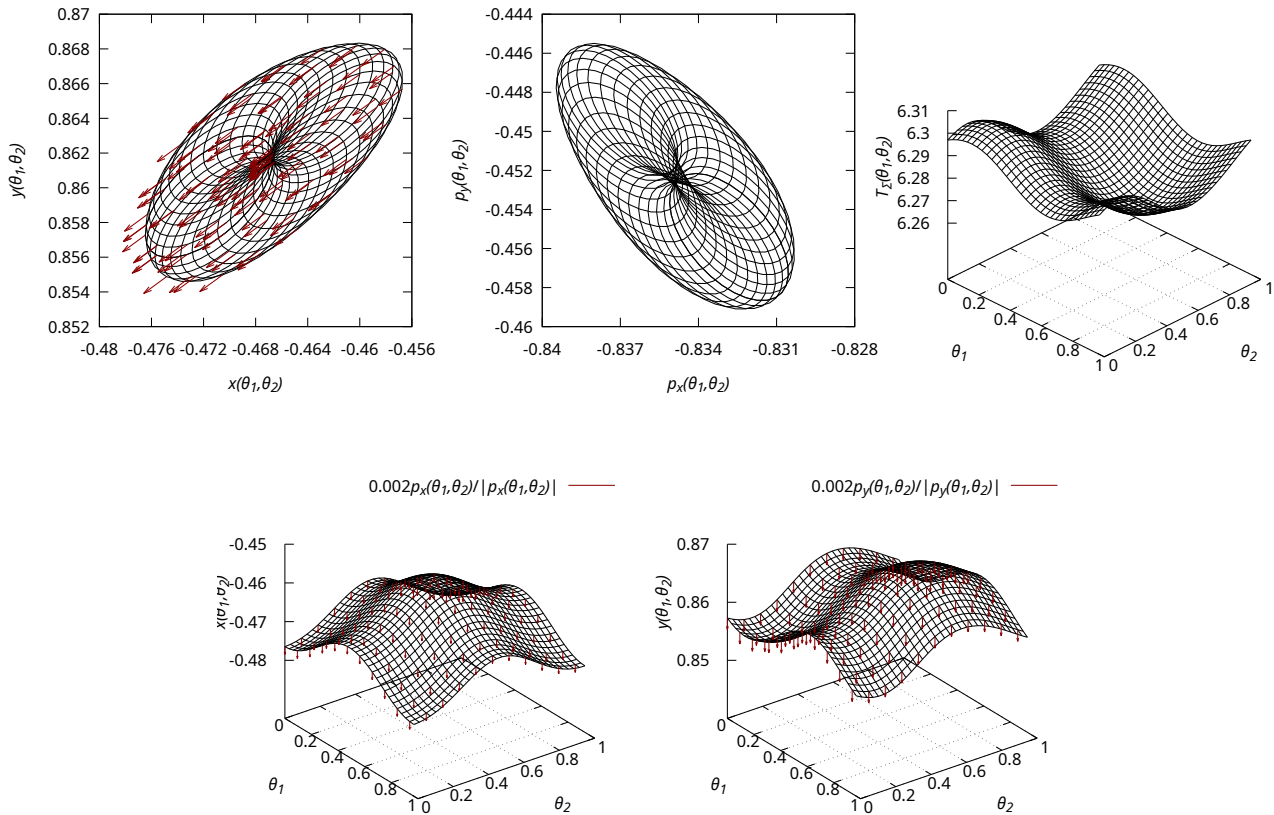


Figure 8: (1,1-2) and (2,1-2): Plots of the 2-D torus for the torus (r_*, r_*) , the red vectors are scaled unit vector to indicate the direction of time at that point. (1,3): Return time surface of the 2-D torus.

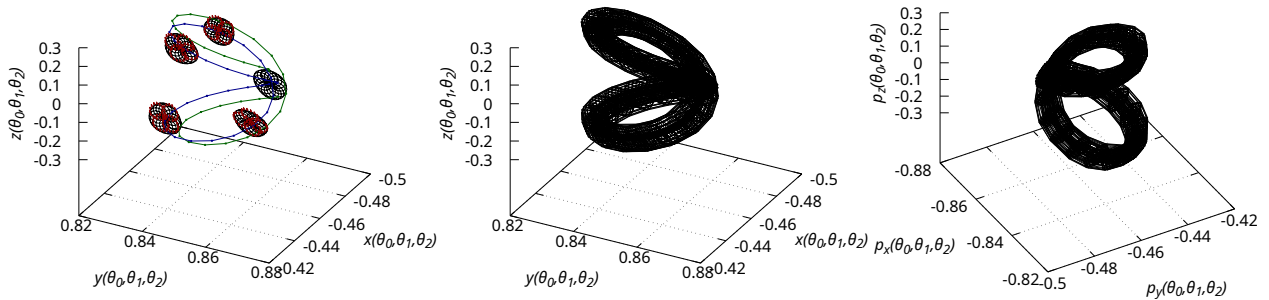


Figure 9: (1,1): Slices of the full torus of $(\omega_0, \omega_1, \omega_2)$ with two trajectories from Σ to itself. (1,2-3): 3-D plots for the variables (x, y, z) and (p_x, p_y, p_z) respectively.

Acknowledgements

The project has been supported with the Spanish grant PID2021-125535NB-I00 (MICINN/AEI/FEDER, UE) and the Catalan grant 2021 SGR 01072. The project that gave rise to these results also received the support of the fellowship from “La Caixa” Foundation (ID 100010434), the fellowship code is LCF/BQ/PR23/11980047. This work has been also funded through the Severo Ochoa and María de Maeztu Program for Centers and Units of Excellence in R&D (CEX2020-001084-M). AJ has also been supported by the Air Force Office of Scientific Research under award number FA8655-24-1-7059. MJC has also been supported by the Spanish grant PID2020-118281GB-C31 (MICINN/AEI/FEDER, UE).

Statements and Declarations

The authors declare no conflict of interests.

References

- [ABBR12] A. Abad, R. Barrio, F. Blesa, and M. Rodríguez. Algorithm 924: TIDES, a Taylor series Integrator for Differential EquationS. *ACM Trans. Math. Software*, 39(1):Art. 5, 28, 2012.
- [And02] M. Andreu. Dynamics in the center manifold around L_2 in the quasi-bicircular problem. *Celestial Mech.*, 84(2):105–133, 2002.
- [AP95] A. Ambrosetti and G. Prodi. *A Primer of Nonlinear Analysis*. Cambridge Studies in Advanced Mathematics. Cambridge University Press, Cambridge, 1995.
- [Arn78] V. Arnold. *Mathematical Methods of Classical Mechanics*. Springer, New York, 1978.
- [Arn83] V. I. Arnold. *Geometrical methods in the theory of ordinary differential equations*, volume 250 of *Grundlehren der Mathematischen Wissenschaften*. Springer-Verlag, New York-Berlin, 1983. Translated from the Russian by Joseph Szücs.
- [Bir27] G. Birkhoff. *Dynamical systems*. Amer. Math. Soc. Publ., 1927.
- [BK78] R. P. Brent and H. T. Kung. Fast algorithms for manipulating formal power series. *J. Assoc. Comput. Mach.*, 25(4):581–595, 1978.
- [Bro79] M. D. Bronštejn. Smoothness of roots of polynomials depending on parameters. *Sibirsk. Mat. Zh.*, 20(3):493–501, 690, 1979.
- [Bru88] A. Bruno. The normal form of a Hamiltonian system. *Russian Math. Surveys*, 43(1):25–66, 1988.
- [CFdlL05] X. Cabré, E. Fontich, and R. de la Llave. The parameterization method for invariant manifolds. III. Overview and applications. *J. Differential Equations*, 218(2):444–515, 2005.
- [DB08] G. Dahlquist and A. k. Björck. *Numerical methods in scientific computing. Vol. I*. Society for Industrial and Applied Mathematics (SIAM), Philadelphia, PA, 2008.
- [Ehr51] C. Ehresmann. Les prolongements d’une variété différentiable. I. Calcul des jets, prolongement principal. II. L’espace des jets d’ordre r de V_n dans V_m . III. Transitivité des prolongements. *C. R. Acad. Sci., Paris*, 233:598–600, 777–779, 1081–1083, 1951.
- [FdIL92] C. Falcolini and R. de la Llave. Numerical calculation of domains of analyticity for perturbation theories in the presence of small divisors. *J. Statist. Phys.*, 67(3-4):645–666, 1992.
- [GC91] A. Griewank and G. Corliss, editors. *Automatic Differentiation of Algorithms: Theory, Implementation, and Application*. SIAM, Philadelphia, Penn., 1991.
- [GJ01] F. Gabern and À. Jorba. A restricted four-body model for the dynamics near the Lagrangian points of the Sun-Jupiter system. *Discrete Contin. Dyn. Syst. Ser. B*, 1(2):143–182, 2001.
- [GJ04] F. Gabern and À. Jorba. Generalizing the Restricted Three-Body Problem. The Bianular and Tricircular Coherent Problems. *Astron. Astrophys.*, 420:751–762, 2004.

- [GJ05] F. Gabern and À. Jorba. Effective computation of the dynamics around a two-dimensional torus of a Hamiltonian system. *J. Nonlinear Sci.*, 15(3), 2005.
- [GJJC⁺23] J. Gimeno, À. Jorba, M. Jorba-Cuscó, N. Miguel, and M. Zou. Numerical integration of high-order variational equations of ODEs. *Appl. Math. Comput.*, 442:127743, 2023.
- [GJL05] F. Gabern, À. Jorba, and U. Locatelli. On the construction of the Kolmogorov normal form for the Trojan asteroids. *Nonlinearity*, 18(4):1705–1734, 2005.
- [GJMS93] G. Gómez, À. Jorba, J. Masdemont, and C. Simó. Study of Poincaré Maps for Orbits near Lagrangian Points. ESOC contract 9711/91/D/IM(SC), final report, European Space Agency, 1993. Reprinted as *Dynamics and mission design near libration points. Vol. IV, Advanced methods for triangular points*, volume 5 of World Scientific Monograph Series in Mathematics, 2001.
- [GJNO22] J. Gimeno, À. Jorba, B. Nicolás, and E. Olmedo. Numerical Computation of High-Order Expansions of Invariant Manifolds of High-Dimensional Tori. *SIAM J. Appl. Dyn. Syst.*, 21(3):1832–1861, 2022.
- [GJZ22] J. Gimeno, À. Jorba, and M. Zou. Taylor package, version 2, 2022.
- [HCL⁺16] À. Haro, M. Canadell, A. Luque, J.-M. Mondelo, and J.-L. Figueras. *The Parameterization Method for Invariant Manifolds. From Rigorous Results to Effective Computations*, volume 195 of *Applied Mathematical Sciences*. Springer-Verlag, 2016.
- [HH64] M. Hénon and C. Heiles. The applicability of the third integral of motion: Some numerical experiments. *Astronom. J.*, 69:73–79, 1964.
- [JJCR20] À. Jorba, M. Jorba-Cuscó, and J. J. Rosales. The vicinity of the Earth-Moon L_1 point in the bicircular problem. *Celest. Mech. Dyn. Astron.*, 132(2):Paper No. 11, 25, 2020.
- [JN21] À. Jorba and B. Nicolás. Using invariant manifolds to capture an asteroid near the L_3 point of the Earth-Moon bicircular model. *Commun. Nonlinear Sci. Numer. Simul.*, 102:105948, 2021.
- [JV97] À. Jorba and J. Villanueva. On the normal behaviour of partially elliptic lower dimensional tori of Hamiltonian systems. *Nonlinearity*, 10:783–822, 1997.
- [JV98] À. Jorba and J. Villanueva. Numerical computation of normal forms around some periodic orbits of the Restricted Three Body Problem. *Phys. D*, 114(3-4):197–229, 1998.
- [JZ05] À. Jorba and M. Zou. A software package for the numerical integration of ODEs by means of high-order Taylor methods. *Exp. Math.*, 14(1):99–117, 2005.
- [Kat66] T. Kato. *Perturbation theory for linear operators*. Die Grundlehren der mathematischen Wissenschaften, Band 132. Springer-Verlag New York, Inc., New York, 1966.
- [Knu98] D. E. Knuth. *The Art of Computer Programming, Volume 2: Seminumerical Algorithms*. Addison-Wesley, Boston, third edition, 1998.
- [Kol54] A. Kolmogorov. On the persistence of conditionally periodic motions under a small change of the Hamilton function. *Dokl. Acad. Nauk. SSSR*, 98(4):527–530, 1954.
- [Mos68] J. Moser. Lectures on Hamiltonian Systems. *Mem. Amer. Math. Soc.*, 81, 1968. 60 pp.
- [Mur20] A. Murillo. Study of volume-preserving flows guided by the Michelson system. Master’s thesis, Univ. Barcelona, 2020.
- [PF23] P. Pita-Forrier. Jet transport for general linear methods. Master’s thesis, Univ. Barcelona, 2023.
- [Poi99] H. Poincaré. *Les méthodes nouvelles de la mécanique céleste*, volume 1, 2, 3. Gauthier-Villars, Paris, 1892–1899.
- [PP15] D. Pérez-Palau. *Dynamical Transport Mechanisms in Celestial Mechanics and Astrodynamics Problem*. PhD thesis, Univ. Barcelona, 2015.
- [Ric80] D. Richardson. A note on a Lagrangian formulation for motion about the collinear points. *Celestial Mech.*, 22(3):231–236, 1980.
- [RJJC21a] J. J. Rosales, À. Jorba, and M. Jorba-Cuscó. Families of halo-like invariant tori around L_2 in the Earth-Moon bicircular problem. *Celest. Mech. Dyn. Astron.*, 133(4):Paper No. 16, 30, 2021.

- [RJJC21b] J. J. Rosales, À. Jorba, and M. Jorba-Cuscó. Transfers from the earth to L_2 halo orbits in the earth-moon bicircular problem. *Celest. Mech. Dyn. Astron.*, 133(11-12):Paper No. 55, 20, 2021.
- [RJJC23] J. J. Rosales, À. Jorba, and M. Jorba-Cuscó. Invariant manifolds near L_1 and L_2 in the quasi-bicircular problem. *Celest. Mech. Dyn. Astron.*, 135(2):Paper No. 15, 47, 2023.
- [Sun85] J. G. Sun. Eigenvalues and eigenvectors of a matrix dependent on several parameters. *J. Comput. Math.*, 3(4):351–364, 1985.
- [Sun90] J. G. Sun. Multiple eigenvalue sensitivity analysis. *Linear Algebra Appl.*, 137/138:183–211, 1990.
- [Sze67] V. Szebehely. *Theory of Orbits: The Restricted Problem of Three Bodies*. Academic Press, 1967.
- [Tha66] H. C. Thacher, Jr. Solution of transcendental equations by series reversion. *Comm. ACM*, 9:10–11, 1966.
- [Wil65] J. H. Wilkinson. *The algebraic eigenvalue problem*. Clarendon Press, Oxford, 1965.